Article

Cancer SLC43A2 alters T cell methionine metabolism and histone methylation

https://doi.org/10.1038/s41586-020-2682-1

Received: 28 July 2019

Accepted: 29 May 2020

Published online: 2 September 2020

Check for updates

Yingjie Bian[1,2,16], Wei Li[1,2,16], Daniel M. Kremer[3], Peter Sajjakulnukit[3], Shasha Li[1,2,4], Joel Crespo[1,2], Zeribe C. Nwosu[3], Li Zhang[3], Arkadiusz Czerwonka[5], Anna Pawłowska[6], Houjun Xia[1,2], Jing Li[1,2], Peng Liao[1,2], Jiali Yu[1,2], Linda Vatan[1,2], Wojciech Szeliga[1,2], Shuang Wei[1,2], Sara Grove[1,2], J. Rebecca Liu[7], Karen McLean[7], Marcin Cieslik[4,8], Arul M. Chinnaiyan[8,9,10,11], Witold Zgodziński[12], Grzegorz Wallner[12], Iwona Wertel[6], Karolina Okła[6], Ilona Kryczek[1,2], Costas A. Lyssiotis[3,13,14,15] & Weiping Zou[1,2,8,14,15] ✉

Abnormal epigenetic patterns correlate with effector T cell malfunction in tumours[1–4], but the cause of this link is unknown. Here we show that tumour cells disrupt methionine metabolism in CD8$^+$ T cells, thereby lowering intracellular levels of methionine and the methyl donor *S*-adenosylmethionine (SAM) and resulting in loss of dimethylation at lysine 79 of histone H3 (H3K79me2). Loss of H3K79me2 led to low expression of STAT5 and impaired T cell immunity. Mechanistically, tumour cells avidly consumed methionine and outcompeted T cells for methionine by expressing high levels of the methionine transporter SLC43A2. Genetic and biochemical inhibition of tumour SLC43A2 restored H3K79me2 in T cells, thereby boosting spontaneous and checkpoint-induced tumour immunity. Moreover, methionine supplementation improved the expression of H3K79me2 and STAT5 in T cells, and this was accompanied by increased T cell immunity in tumour-bearing mice and patients with colon cancer. Clinically, tumour SLC43A2 correlated negatively with T cell histone methylation and functional gene signatures. Our results identify a mechanistic connection between methionine metabolism, histone patterns, and T cell immunity in the tumour microenvironment. Thus, cancer methionine consumption is an immune evasion mechanism, and targeting cancer methionine signalling may provide an immunotherapeutic approach.

Immune checkpoint blockade therapies have demonstrated unprecedented clinical efficacy in cancer treatment, but their application has been hindered by therapeutic resistance[5]. CD8$^+$ T cells mediate anti-tumour immunity. Unfortunately, tumour-infiltrating CD8$^+$ T cells are often dysfunctional (this is known as T cell exhaustion)[1,6]. Differentiation and activation of T cells are associated with changes to the epigenetic landscape at gene loci that encode effector molecules, including interferon (IFN) and granzyme B[4,7]. However, these dynamic epigenetic changes in T cells may be disrupted by tumour cells[2,4,8] via metabolic regulation in the tumour microenvironment[9–12]. Tumour-intrinsic mechanisms, and oncogenic signalling in particular, may contribute to abnormal tumour metabolism[13,14]. However, it is unclear whether amino acid metabolism can affect the T cell epigenetic landscape and in turn alter T cell function in tumours.

Tumour cells outcompete T cells for methionine

Exhausted T cells exhibit distinct histone profiles and limit tumour immunotherapy[2,3]. To test whether abnormal amino acid metabolism is related to alterations in histones and dysfunction in T cells, we cultured mouse CD8$^+$ T cells without individual amino acids. Omission of methionine resulted in the most marked T cell death and dysfunction, as shown by staining of cultured cells for the apoptosis marker annexin V and the effectors IFNγ and TNFα (Fig. 1a–c). Thus, access to methionine is critical for the survival and function of T cells.

Next, we tested whether tumour cells impaired CD8$^+$ T cell function by altering methionine levels. We cultured ID8 (Fig. 1d) and B16F10 (Fig. 1e) tumour cells with medium containing 20–100 μM methionine. Regardless of methionine concentrations, fresh medium had a minimal effect

[1]Department of Surgery, University of Michigan School of Medicine, Ann Arbor, MI, USA. [2]Center of Excellence for Cancer Immunology and Immunotherapy, University of Michigan Rogel Cancer Center, University of Michigan School of Medicine, Ann Arbor, MI, USA. [3]Department of Molecular and Integrative Physiology, University of Michigan Medical School, Ann Arbor, MI, USA. [4]Department of Computational Medicine & Bioinformatics, University of Michigan, Ann Arbor, MI, USA. [5]Department of Virology and Immunology, Maria Curie-Skłodowska University, Lublin, Poland. [6]First Chair and Department of Oncological Gynecology and Gynecology, Medical University of Lublin, Lublin, Poland. [7]Department of Obstetrics and Gynecology, University of Michigan, Ann Arbor, MI, USA. [8]Department of Pathology, University of Michigan, Ann Arbor, MI, USA. [9]Department of Urology, University of Michigan, Ann Arbor, MI, USA. [10]Michigan Center for Translational Pathology, University of Michigan, Ann Arbor, MI, USA. [11]Howard Hughes Medical Institute, University of Michigan, Ann Arbor, MI, USA. [12]Second Department of General, Gastrointestinal Surgery and Surgical Oncology of the Alimentary Tract, Medical University of Lublin, Lublin, Poland. [13]Department of Internal Medicine, University of Michigan Medical School, Ann Arbor, MI, USA. [14]Graduate Program in Immunology, University of Michigan School of Medicine, Ann Arbor, MI, USA. [15]Graduate Program in Cancer Biology, University of Michigan School of Medicine, Ann Arbor, MI, USA. [16]These authors contributed equally: Yingjie Bian, Wei Li. ✉e-mail: wzou@med.umich.edu

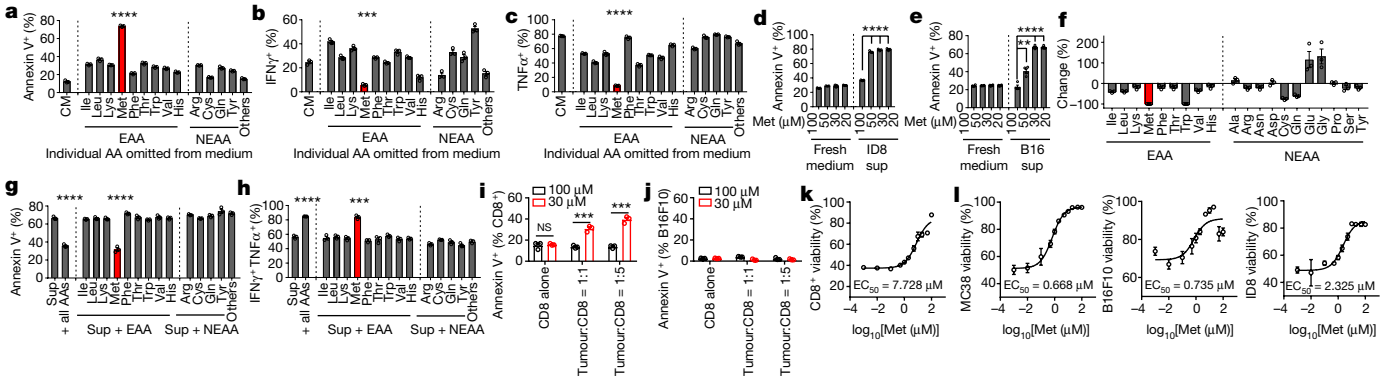

Fig. 1 | Tumour cells outcompete T cells for methionine to impair T cell function. a–**c**, Effects of amino acids on T cell apoptosis (**a**) and effector cytokines (**b**, **c**). Activated mouse CD8$^+$ T cells were cultured with complete medium (CM) or media from which individual amino acids (AAs) had been omitted for 36 h. EAA, essential amino acid; NEAA, non-essential amino acid. **d**, **e**, Effect of tumour cell culture supernatants on T cell apoptosis. CD8$^+$ T cells were cultured for 36 h with supernatants (sup) from cultured ID8 (**d**) or B16F10 (**e**) cells with varying concentrations of methionine (Met). **f**, Mass spectrometry (MS) detection of amino acid consumption by cultured tumour cells (bars show change from fresh medium). **g**, **h**, Effect of amino acid supplementation in tumour cell supernatant on T cell apoptosis (**g**) and cytokine production (**h**). CD8$^+$ T cells were cultured with B16F10 cell culture supernatant supplemented with amino acids for 36 h. **i**, **j**, Apoptosis of T cells (**i**) and tumour cells (**j**) induced by methionine competition. B16F10 cells and CD8$^+$ T cells were cultured at different ratios for 72 h in a Transwell system with 30 or 100 μM methionine. NS, not significant. **k**, **l**, Effect of methionine on viability of CD8$^+$ T cells (**k**) and tumour cells (**l**). Data are mean ± s.e.m. Sample sizes (*n*), *P* values, statistical tests and numbers of replications are listed in 'Statistics and reproducibility' (Methods).

on apoptosis in T cells (Fig. 1d, e). However, supernatant from cultured ID8 (Fig. 1d) or B16F10 cells (Fig. 1e) induced apoptosis in CD8$^+$ T cells when the original culture medium had contained less than 100 μM methionine. We obtained similar results when we cultured mouse CD8$^+$ T cells with the supernatant from MC38 or CT26 colon cancer cells (Extended Data Fig. 1a, b) or human CD8$^+$ T cells with the supernatant from A375 melanoma cells (Extended Data Fig. 1c). Moreover, supernatants from tumour cell cultures increased death and dysfunction in cultured ID8 tumour-infiltrating T cells (Extended Data Fig. 1d, e). Thus, tumour cells limit T cell access to methionine and impair T cell survival and function.

The physiological concentration of methionine in human serum is about 30 μM[15,16], but serum methionine was lower in patients with cancer than in healthy donors (Extended Data Fig. 1f, g). To evaluate methionine consumption within the physiological range, we cultured B16F10 cells with 30 μM methionine and analysed the abundance of amino acids in the supernatant. Tumour cells consumed the majority of amino acids, including methionine and tryptophan (Fig. 1f, Extended Data Fig. 1h). We subsequently cultured mouse CD8$^+$ T cells in B16F10 cell supernatants supplemented with individual amino acids. Among all amino acids, only methionine supplementation prevented T cell apoptosis and rescued the production of IFNγ and TNFα (Fig. 1g, h). We obtained similar results with human CD8$^+$ T cells (Extended Data Fig. 1i, j). Tumour glycolysis regulates T cell function[17], so we cultured T cells in tumour cell supernatant supplemented with glucose or methionine. Methionine, but not glucose, restored T cell survival and production of cytokines (Extended Data Fig. 1k–m). Moreover, simultaneous supplementation with glucose and methionine did not enhance this effect. Thus, consumption of methionine by tumour cells impairs T cell survival and function.

We cultured B16F10 and CD8$^+$ T cells in a Transwell system (Extended Data Fig. 1n). A high concentration of methionine (100 μM) had a minimal effect on apoptosis in tumour or CD8$^+$ T cells. However, a low concentration of methionine (30 μM) caused apoptosis in CD8$^+$ T cells (Fig. 1i), but not tumour cells (Fig. 1j). Then, we evaluated the half-maximal effective concentration (EC_{50}) of methionine to maintain CD8$^+$ T and tumour cell viabilities. Both mouse and human CD8$^+$ T cells were more sensitive than tumour cells to methionine deprivation, as shown by their different EC_{50} values (Fig. 1k, l, Extended Data Fig. 1o, p). Thus, tumour cells outcompete T cells for methionine, thereby impairing T cell survival and function.

Low methionine decreases H3K79me2 in T cells

To investigate the mechanism by which tumour cells affected CD8$^+$ T cells through methionine deprivation, we performed RNA sequencing (RNA-seq) on CD8$^+$ T cells cultured with fresh medium, B16F10 supernatant, and supernatant plus methionine (Extended Data Fig. 2a). Network grouping analysis revealed that pathways related to metabolism, function, and survival were affected by tumour supernatants (Extended Data Fig. 2b). Correspondingly, gene set enrichment analysis (GSEA) showed an enrichment in the T cell apoptosis signature and poor T cell receptor signalling in the presence of tumour supernatant (Fig. 2a), whereas methionine supplementation largely rescued this phenotype (Extended Data Fig. 2c). Moreover, one-carbon metabolic process and the methionine cycle were defective in CD8$^+$ T cells cultured with supernatant (Fig. 2b), and were restored by methionine addition (Extended Data Fig. 2d, e).

Next, we performed a metabolomics analysis of parallel CD8$^+$ T cells. We observed obvious metabolic changes in T cells cultured with tumour supernatants, and these too were rescued by methionine addition (Extended Data Fig. 2f). We specifically examined metabolites related to the one-carbon process and the methionine cycle (Fig. 2c, Extended Data Fig. 2g), and found that CD8$^+$ T cells cultured in tumour supernatant showed a marked decrease in intracellular methionine, SAM and *S*-adenosyl-homocysteine (SAH) (Fig. 2d–f). Supplementation with methionine restored intracellular methionine, SAM, and SAH (Fig. 2d–f), and induced a decrease in serine and L-cystathionine (Extended Data Fig. 2h, i). To test which metabolite was the key factor, we cultured CD8$^+$ T cells with tumour supernatant supplemented with methionine, SAM, SAH, or L-cystathionine. Supplementation with methionine or SAM prevented CD8$^+$ T cell apoptosis, and rescued the T cell cytokine profile (Fig. 2g, h).

Intracellular methionine is converted into SAM, the donor for epigenetic methylation[18,19]. Thus, we tested T cell histone marks and found that supernatants induced a marked decrease in H3K79me2, but not in other marks (Fig. 2i). Similar results were obtained in mouse CD8$^+$ T cells cultured with CT26 or MC38 supernatant and in human CD8$^+$ T cells

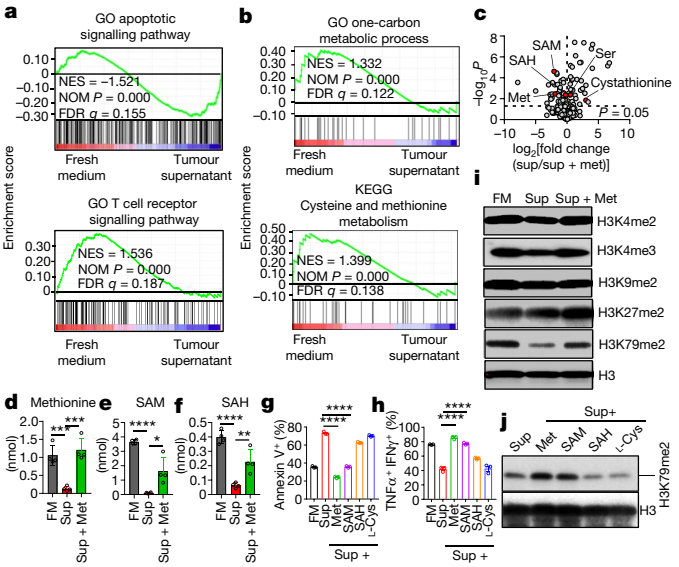

Fig. 2 | Tumour cells alter CD8⁺ T cell methionine metabolism to diminish H3K79me2. a, **b**, GSEA plot showing enriched apoptotic and TCR signalling pathways (**a**) and defective methionine metabolism signalling (**b**) in CD8⁺ T cells cultured in tumour cell culture supernatant. GO, gene ontology; KEGG, Kyoto Encyclopedia of Genes and Genomes; NES, normalized enrichment score. **c**–**f**, Changes to the methionine metabolism pathway in CD8⁺ T cells cultured with fresh medium (FM), tumour cell supernatant, or supernatant supplemented with methionine. **c**, Volcano plot shows changes in metabolite levels between T cells cultured with supernatant and those cultured with supernatant and methionine. Intracellular methionine (**d**), SAM (**e**), and SAH concentrations (**f**) were detected by MS. **g**, **h**, Effect of metabolite supplementation on apoptosis (**g**) and cytokine production (**h**) in CD8⁺ T cells cultured in tumour cell supernatant. **i**, Effect of tumour supernatants on histone methylation in CD8⁺ T cells. **j**, Effect of methionine metabolite supplementation on H3K79 methylation in CD8⁺ T cells. Data are mean ± s.e.m. Sample sizes (*n*), *P* values, statistical tests and numbers of replications are listed in 'Statistics and reproducibility' (Methods).

cultured with A375 supernatants (Extended Data Fig. 2j, k). Moreover, the reduced H3K79me2 could be recovered by supplementation with methionine or SAM, but not SAH or L-cystathionine (Fig. 2j). Thus, methionine restriction by tumour cells reduces the methyl donor SAM and, in turn, impairs H3K79me2 in CD8⁺ T cells.

Loss of H3K79me2 impairs STAT5 expression

Disruptor of telomeric silencing 1-like (DOT1L) is the specific and sole methyltransferase for H3K79[20,21]. We cultured CD8⁺ T cells with EPZ004777, an inhibitor of DOT1L. EPZ004777 inhibited H3K79me2, induced CD8⁺ T cell apoptosis, and suppressed CD8⁺ T cell cytokine expression in a dose-dependent manner (Fig. 3a–c). To genetically explore the role of H3K79me2 in T cell function, we crossed conditional *Dot1l* allele (*Dot1l*$^{flox/flox}$, referred to here as *Dot1l*$^{+/+}$) mice[22] with CD4-Cre transgenic mice to delete *Dot1l* specifically in T cells (referred to here as *Dot1l*$^{-/-}$ mice) (Extended Data Fig. 3a). Deletion of *Dot1l* led to a loss of H3K79me2 in CD8⁺ T cells (Fig. 3d, Extended Data Fig. 3b) and resulted in increased apoptosis, especially upon activation (Fig. 3e). Moreover, intracellular cytokine staining showed impaired function in *Dot1l*$^{-/-}$ CD8⁺ T cells (Fig. 3f). RNA array analysis showed that *Dot1l*$^{-/-}$ CD8⁺ T cells (Extended Data Fig. 3c) were similar to T cells exposed to methionine deficiency (Extended Data Fig. 2b). For instance, like methionine-deficient T cells (Fig. 2a), *Dot1l*$^{-/-}$ T cells showed an enriched apoptotic gene signature and impaired T cell receptor functional gene signature (Extended Data Fig. 3d, e). The data suggest that T cell malfunctions caused by methionine deficiency or by impaired DOT1L-dependent histone methylation share a mechanism.

We assessed the role of T cell DOT1L in tumour immunity and found that MC38 tumours grew faster in *Dot1l*$^{-/-}$ mice than in *Dot1l*$^{+/+}$ mice (Fig. 3g, h). Correspondingly, *Dot1l*$^{-/-}$ mice showed an increase in CD8⁺ T cell apoptosis in tumour draining lymph nodes and tumour tissues (Fig. 3i), as well as a decrease in secretion of TNFα, IFNγ, and granzyme B from tumour-infiltrating CD8⁺ T cells (Extended Data Fig. 3f). In addition, PD-L1 blockade inhibited tumour growth in *Dot1l*$^{+/+}$ mice but not in *Dot1l*$^{-/-}$ mice (Extended Data Fig. 3g). We obtained similar results with B16F10 tumours (Extended Data Fig. 3h, i). To confirm that the positive role of methionine in T cells depends on DOT1L, we cultured *Dot1l*$^{+/+}$ and *Dot1l*$^{-/-}$ T cells with methionine supplementation in the presence of tumour supernatant. Methionine supplementation failed to protect *Dot1l*$^{-/-}$ T cells from apoptosis (Fig. 3j) or to rescue their impaired cytokine production (Fig. 3k). Thus, loss of DOT1L, which mediates H3K79me2, weakens anti-tumour T cell immunity.

We next investigated how loss of H3K79me2 results in T cell dysfunction. *Dot1l*$^{-/-}$ CD8⁺ T cells showed enrichment of an apoptosis gene signature (Fig. 3l, Extended Data Fig. 3c, d). The JAK–STAT pathway regulates T cell survival and effector function[23]. Among components of the JAK–STAT pathway, expression of *Stat5* was most strongly affected by H3K79me2 deficiency (Fig. 3m, Extended Data Fig. 3j); both total STAT5 and phosphorylated STAT5 (p-STAT5), but not other STATs, were reduced in *Dot1l*$^{-/-}$ T cells (Fig. 3n). In mouse CD8⁺ T cells cultured with B16F10 supernatant, *Stat5* transcripts (Extended Data Fig. 3k), total STAT5 and p-STAT5 (Fig. 3o) were all reduced. These effects were reversed by supplementation with methionine or SAM, but not SAH or L-cystathionine (Fig. 3o). Moreover, RNA-seq data from human CD8⁺ T cells treated with the DOT1L inhibitor SGC0946[24] showed reduced *STAT5* expression, enriched apoptotic gene signatures, and impaired T cell signalling (Extended Data Fig. 3l–n). Thus, tumour cells outcompete T cells for methionine, resulting in a reduction in H3K79me2 and defective STAT5 signalling in CD8⁺ T cells.

H3K79me2 is an active gene mark in mammalian cells and occurs on the promoter and 5′ regions within the coding regions of transcriptionally active genes[25,26]. Chromatin immunoprecipitation and sequencing (ChIP–seq) data[27,28] revealed high H3K79me2 occupancy in the key regulatory regions of the *STAT5B* promoter in mouse and human (Extended Data Fig. 3o, p). ChIP analysis demonstrated high levels of H3K79me2 on the *Stat5* promoter (Fig. 3p, Extended Data Table 1). This binding was diminished in T cells cultured with B16F10 supernatants and restored by methionine supplementation (Fig. 3q). Thus, H3K79me2 is involved in the direct regulation of STAT5 transcription in CD8⁺ T cells.

Methionine restores T cell immunity

To demonstrate the relevance of methionine competition between tumour cells and T cells in vivo, we conducted four complementary studies. First, we found that tumour-infiltrating CD8⁺ T cells harboured lower levels of H3K79me2 and STAT5 than did T cells in the draining lymph nodes and spleen (Extended Data Fig. 4a–d).

Second, we confirmed that human tumour-infiltrating CD8⁺ T cells from ovarian carcinoma omentum, malignant ascites, and several other cancers showed a decrease in H3K79me2 and STAT5 compared to peripheral T cells (Extended Data Fig. 4e–i). To examine the effect of methionine on human-tumour infiltrating T cells, we cultured human colorectal cancer-infiltrating T cells with or without methionine. The addition of methionine enhanced the expression of T cell effector cytokines, H3K79me2, and STAT5 (Extended Data Fig. 4j–m).

Third, we injected methionine into B16F10 tumours in mice. Methionine supplementation delayed tumour growth, enhanced H3K79me2 and STAT5 expression in tumour-infiltrating CD8⁺ T cells, and increased T cell survival and expression of polyfunctional cytokines (Fig. 4a–e). Injections of methionine into ID8 tumours in mice also slowed down

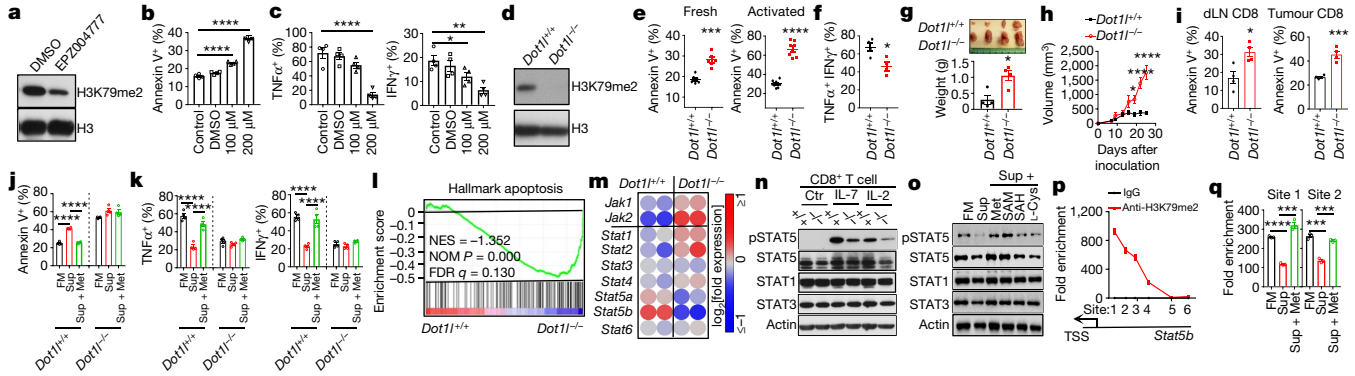

Fig. 3 | Loss of H3K79me2 impairs T cell anti-tumour immunity through STAT5. a–**c**, CD8$^+$ T cells were treated with EPZ004777 or vehicle (DMSO) for 48 h. Western blot (**a**) shows H3K79me2 in CD8$^+$ T cells. Fluorescence-activated cell sorting was used to measure apoptosis (**b**) and cytokine production (**c**). **d**, Western blot shows H3K79me2 in *Dot1l*$^{+/+}$ and *Dot1l*$^{-/-}$ CD8$^+$ T cells. **e**, **f**, Effect of DOT1L deletion on apoptosis (**e**) and cytokine production (**f**) in CD8$^+$ T cells. **g**–**i**, Effect of T cell DOT1L deficiency on MC38 growth (**g** (day 25), **h**) and T cell viability in draining lymph nodes (dLN) and tumour (**i**). **j**, **k**, Effect of methionine supplementation on apoptosis (**j**) and cytokine production (**k**) in *Dot1l*$^{+/+}$ and *Dot1l*$^{-/-}$ CD8$^+$ T cells. **l**, GSEA plot shows enriched apoptotic pathway genes in *Dot1l*$^{-/-}$ CD8$^+$ T cells. **m**, Heat map shows mRNA levels for components of the JAK–STAT pathway in mouse *Dot1l*$^{-/-}$ and *Dot1l*$^{+/+}$ CD8$^+$ T cells. **n**, Western blot shows STAT5 and p-STAT5 in *Dot1l*$^{+/+}$ (+/+) and *Dot1l*$^{-/-}$ (−/−) CD8$^+$ T cells. **o**, Western blot shows STAT5 and p-STAT5 in CD8$^+$ T cells cultured with fresh medium, tumour cell supernatant, or supernatant supplemented with different metabolites. **p**, ChIP assay shows H3K79me2 occupancy on the *Stat5b* promoter in CD8$^+$ T cells. TSS, transcription start site. **q**, ChIP assay shows H3K79me2 occupancy on the *Stat5b* promoter in CD8$^+$ T cells cultured with fresh medium, tumour cell supernatant, or supernatant supplemented with different metabolites. Data are mean ± s.e.m. Sample sizes (*n*), *P* values, statistical tests and numbers of replications are listed in 'Statistics and reproducibility' (Methods).

tumour progression (Fig. 4f), enhanced T cell (but not tumour cell) survival (Extended Data Fig. 4n), and increased effector cytokine levels in tumour ascites and tumour-infiltrating CD8$^+$ T cells (Fig. 4g, h). After methionine supplementation by injection, we detected high levels of methionine in ID8 ascites (Extended Data Fig. 4o). We also treated mice bearing CT26 tumours with methionine, anti-PD-L1, or a combination of both, and found that methionine plus anti-PD-L1 had a synergistic anti-tumour effect, compared to either treatment alone. This was accompanied with increased T cell tumour infiltration and reduced T cell apoptosis (Extended Data Fig. 4p–r).

Fourth, we provided methionine supplementation to patients with colorectal cancer (Extended Data Table 2). Methionine supplementation resulted in an increase in H3K79me2 and p-STAT5 in CD8$^+$ T cells (Fig. 4i), enhanced T cell IL-2 production (Fig. 4j) and CD8$^+$ T cell polyfunctional cytokine expression (Fig. 4k), and decreased CD8$^+$ T cell apoptosis (Fig. 4l) in these patients. Together, our data suggest that methionine deficiency impairs H3K79me2 and STAT5 expression and function in T cells.

Tumour impairs tumour immunity through SLC43A2

Methionine is transported into cells by the solute carrier family (SLC), including system L-type and A-type transporters[29]. We cultured B16F10 cells with BCH (an inhibitor of system L transporters) or MeAIB (an inhibitor of system A transporters)[29]. Then, we cultured CD8$^+$ T cells with the resulting tumour supernatants and analysed CD8$^+$ T cells. BCH, but not MeAIB, prevented T cell apoptosis and rescued the impaired cytokine profile (Extended Data Fig. 5a, b). Thus, system L transporters may be responsible for consumption of methionine by tumours.

Next, we compared the SLC transcripts in effector CD8$^+$ T cells and tumour cells, and found that *SLC7A5* and *SLC43A2* (two system L transporters) were relatively highly expressed on tumour cells (Extended Data Fig. 5c). Western blots revealed minimal SLC43A2 expression in effector CD8$^+$ T cells and comparable SLC7A5 expression in effector CD8$^+$ T cells and several tumour cells (Extended Data Fig. 5d). In line with this, we detected minimal SLC43A2 in human CD8$^+$ T cells, compared to several tumour cells (Extended Data Fig. 5e). The differential SLC43A2 expression in tumour and CD8$^+$ T cells suggests that tumour cells may be well-positioned to outcompete T cells for methionine via SLC43A2.

To test this possibility, we used a short hairpin RNA (shRNA) against *SLC43A2* (sh*SLC43A2*) to knock down *SLC43A2* in B16F10 cells (Extended Data Fig. 5f), which induced a decrease in methionine consumption (Extended Data Fig. 5g). Then, we cultured CD8$^+$ T cells with the tumour supernatants from sh*SLC43A2* cells or from tumour cells expressing scrambled shRNA. CD8$^+$ T cells cultured with supernatant from sh*SLC43A2* cells showed reduced T cell apoptosis and enhanced polyfunctional cytokine expression (Fig. 5a, b). Furthermore, T cells cultured with sh*SLC43A2* cells in a Transwell system (Extended Data Fig. 1n), showed a reduction in apoptosis and an increase in cytokine production (Fig. 5c, d), as well as increased H3K79me2, when compared with T cells cultured with control cells treated with scrambled shRNA (Fig. 5e). Thus, tumour cells outcompete T cells for methionine via SLC43A2, and this affects T cell histone methylation and function.

We next injected B16F10 cells treated with sh*SLC43A2* or scrambled shRNA (control) into *Dot1l*$^{+/+}$ and *Dot1l*$^{-/-}$ C57BL/6 mice. Tumour growth was slower in *Dot1l*$^{+/+}$ mice bearing sh*SLC43A2* B16F10 cells than in those bearing control B16F10 cells (Fig. 5f). However, *SLC43A2* knockdown did not affect tumour progression in *Dot1l*$^{-/-}$ mice (Extended Data Fig. 5h). The data suggest that there is a functional connection between tumour SLC43A2 and T cell DOT1L in anti-tumour immunity. Furthermore, treatment of tumour cells with sh*SLC43A2* did not affect tumour growth in *Rag1*$^{-/-}$ mice (Extended Data Fig. 5i). Thus, tumour immunity contributed to tumour control in sh*SLC43A2*-treated tumours. Consistent with this, tumour T cell infiltration (Extended Data Fig. 5j) and effector molecules were increased in sh*SLC43A2*-treated tumours when compared with control tumours in wild-type C57BL/6 mice (Fig. 5g). Treatment with anti-PD-L1 further inhibited the growth of sh*SLC43A2* B16F10 tumours (Extended Data Fig. 5k).

We also studied mice bearing sh*SLC43A2* ID8 tumours (Extended Data Fig. 5l). As with B16F10 tumours, sh*SLC43A2* had no effect on tumour growth in *Rag1*$^{-/-}$ mice (Extended Data Fig. 5m), but tumour growth was slower and CD8$^+$ T cell infiltration was increased in WT mice bearing sh*SLC43A2* ID8 tumours compared with control ID8 tumours (Extended Data Fig. 5n, o). These data suggest that pharmacologically targeting SLC43A2 may promote anti-tumour immunity. Given that no specific SLC43A2 inhibitor is available, we treated B16F10 tumour-bearing mice with BCH with or without anti-PD-L1 treatment (Fig. 5h). Treatment with BCH or anti-PD-L1 alone partially inhibited

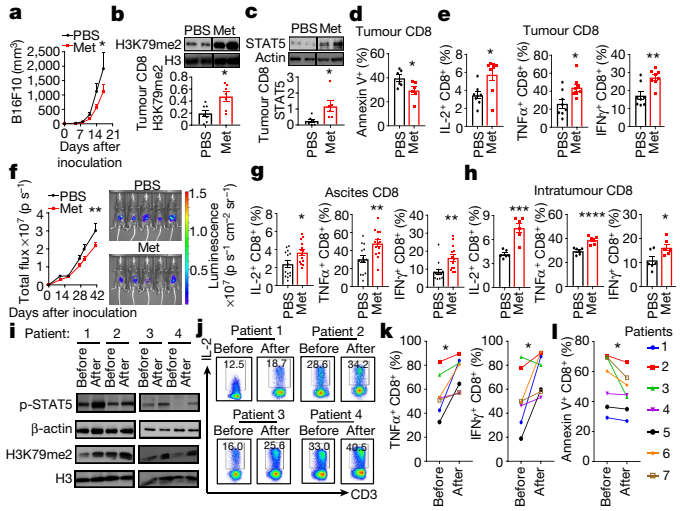

Fig. 4 | Methionine supplementation in tumours restores T cell immunity. **a**–**e**, Methionine supplementation restored T cell immunity in B16F10 tumour-bearing mice. Tumour growth (**a**), and H3K79me2 (**b**) and STAT5 (**c**) in tumour-infiltrating CD8$^+$ T cells, were monitored. FACS was used to measure apoptosis (**d**) and cytokine production (**e**) in intratumour CD8$^+$ T cells. PBS, phosphate-buffered saline (vehicle). **f**–**h**, Methionine supplementation restored T cell immunity in ID8 tumour-bearing mice. Tumour growth was monitored by bioluminescence imaging (**f**). FACS was used to measure cytokine production in CD8$^+$ T cells in the ascites (**g**) and tumours (**h**). **i**–**l**, Studies on patients with colorectal cancer treated with methionine. Western blots show p-STAT5 and H3K79me2 in peripheral CD8$^+$ T cells before and after methionine treatment (**i**). FACS was used to measure IL-2$^+$ T cells (**j**) and effector cytokine production (**k**) and apoptosis (**l**) in CD8$^+$ T cells in patients before and after methionine treatment. Data are mean ± s.e.m. Sample sizes (*n*), *P* values, statistical tests and numbers of replications are listed in 'Statistics and reproducibility' (Methods).

tumour growth, and the combination had a synergistic effect (Fig. 5h). Moreover, the combination treatment induced the highest T cell infiltration (Extended Data Fig. 5p) and the highest expression of effector molecules in tumour-infiltrating CD8$^+$ T cells (Fig. 5i). The combination treatment also synergistically inhibited tumour growth and enhanced cytokine production by tumour-infiltrating CD8$^+$ T cells in mice bearing ID8 tumours (Fig. 5j–l). These results suggest that targeting tumour SLC43A2 in combination with checkpoint blockade may be an effective anti-cancer approach.

Finally, we investigated a potential relationship between tumour SLC43A2 expression, T cell signatures, and clinical outcome in patients with cancer. Using data from the Cancer Genome Atlas (TCGA) database, we found that *SLC43A2* transcripts were higher in tumours than in matched normal tissue (Fig. 5m). Moreover, high tumour SLC43A2 expression was associated with poor survival (Extended Data Fig. 5q–s). Single-cell RNA-seq of tumour-infiltrating T cells and cancer cells from patients with melanoma[30] showed higher *SLC43A2* transcripts in tumour cells than in T cells (Extended Data Fig. 5t). We divided the patients into two groups according to high or low expression of SLC43A2 in tumours. GSEA showed that expression of methionine metabolic signalling genes was enriched in melanoma cells with high levels of SLC43A2 (Extended Data Fig. 5u). Tumour SLC43A2 levels negatively correlated with *CD8* and *IFNG* transcripts in the same tumours (Extended Data Fig. 5v). Furthermore, compared to patients with low tumour SLC43A2 levels, T cells in patients with high tumour SLC43A2 levels showed weak signatures for methionine metabolism and histone methylation, and low expression of effector genes (Extended Data Fig. 5w–y). Thus, high expression of SLC43A2 in tumours is associated with reduced T cell immune responses in patients with cancer.

Discussion

Recent studies have started to explore the roles of amino acids in T cell activation and epigenetic reprogramming[31–33]. Methionine is an essential amino acid, and is converted to SAM for methyltransferases to yield methylated substrates, including histone methylation[18,19]. Hence, SAM provides a link between methionine metabolism and epigenetic regulation. Dysfunctional T cells exhibit a distinct epigenetic landscape including histone alteration[2,3]. Thus, abnormal methionine metabolism may lead to particular histone alteration in T cells and contribute to their dysfunction in the tumour microenvironment.

We have demonstrated direct competition between tumour cells and T cells for methionine, which results in reductions in a series of substrates for one-carbon metabolism, including SAM, in T cells. DOT1L is the only methyltransferase for H3K79[20,21], and has a relatively low Michaelis constant (K_m) for SAM[34]. These characteristics contribute

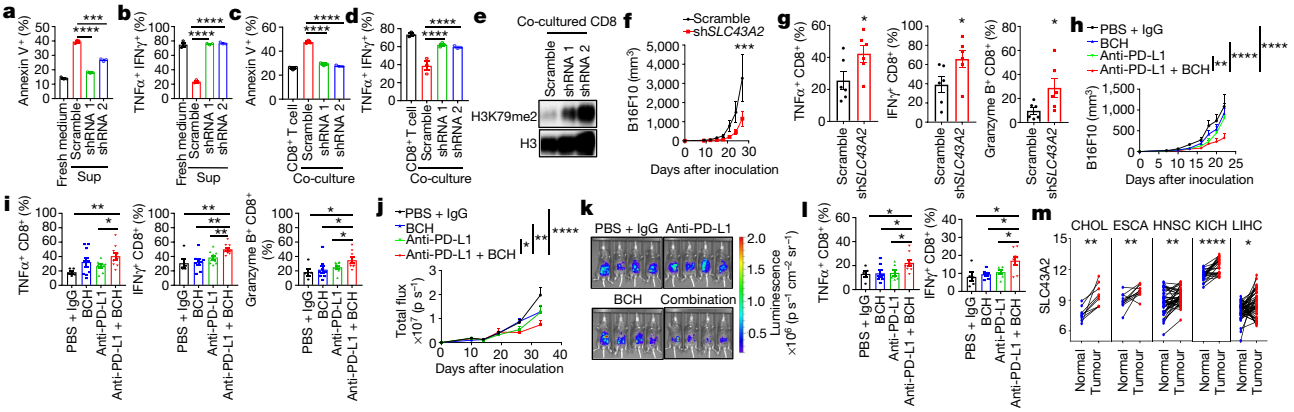

Fig. 5 | Tumour cells outcompete T cells for methionine via SLC43A2. a, **b**, Effects of supernatants from sh*SLC43A2*-treated tumours on T cell apoptosis (**a**) and cytokine production (**b**). Scramble, control; shRNA 1 and shRNA 2, sh*SLC43A2*. **c**–**e**, Effects of tumour *SLC43A2* knockdown on apoptosis (**c**), cytokine production (**d**) and H3K29me2 modification (**e**) in T cells. CD8$^+$ T cells were co-cultured with wild-type and sh*SLC43A2*-treated B16F10 cells in a Transwell system in medium containing 30 μM methionine. Apoptosis (**c**), cytokine production (**d**) and H3K79me2 (**e**) in CD8$^+$ T cells were determined by FACS and western blot after 72 h. **f**, **g**, Effects of tumour *SLC43A2* knockdown on tumour growth (**f**) and tumour T cell function (**g**). **h**–**l**, Effects of a combination of BCH and anti-PD-L1 treatment on B16F10 (**h**, **i**) and ID8 (**j**–**l**) tumour-bearing mice. **h**, **j**, **k**, Tumour growth; **i**, **l**, TNFα$^+$, IFNγ$^+$ and granzyme B$^+$ CD8$^+$ T cells. **m**, *SLC43A2* transcripts in tumours and paired adjacent normal tissue samples for several types of tumour from TCGA. CHOL, cholangiocarcinoma; ESCA, oesophageal carcinoma; HNSC, head and neck squamous cell carcinoma; KICH, kidney chromophobe; LIHC, liver hepatocellular carcinoma. Data are mean ± s.e.m. Sample sizes (*n*), *P* values, statistical tests and numbers of replications are listed in 'Statistics and reproducibility' (Methods).

to the sensitivity of H3K79 methylation to deprivation of methionine and SAM, and explain why T cell H3K79me2 is predominantly sensitive to tumour-altered methionine metabolism. We have also validated the mechanistic connection between methionine, H3K79me2, and STAT5 in human and mouse tumour-infiltrating T cells. Notably, as substantial methionine is required for abnormal tumour cell proliferation and metabolism[35], the effects of dietary methionine restriction on tumour growth have been tested in immune-deficient systems[36]. Our work indicates that both human and mouse effector T cells are sensitive to methionine. Thus, tumour-specific methionine restriction is essential to maintain T cell immunity in patients with cancer.

H3K79me2 is an active transcriptional histone mark[21]. Biochemical and genetic inhibition of DOT1L abolished H3K79me2 and STAT5, resulting in T cell apoptosis and dysfunction. Mechanistically, H3K79me2 controls STAT5 transcription in $CD8^+$ T cells. Thus, we have identified a causal and biological link between a particular histone alteration (H3K79me2) and a transcription factor (STAT5) that is critical for defining T cell phenotype. Moreover, tumour cells outcompete T cells for methionine via SLC43A2, a major methionine transporter. Given that SLC43A2 is highly expressed on multiple human and mouse tumour cells with different genetic backgrounds, abnormal tumour SLC43A2 and its related methionine metabolism are unlikely to be driven by shared key oncogenes. Inhibition of tumour SLC43A2 can normalize methionine metabolism in effector T cells and rescue their function, and can also improve spontaneous and checkpoint blockade-induced anti-tumour immunity in preclinical models. Our work has not only generated insights into SLC biology in T cells, but also identified tumour SLC43A2 as an mechanism of immunotherapy resistance in patients with cancer. Indeed, we have established a negative correlation between tumour cell SLC43A2 levels, histone methylation in tumour-infiltrating T cells, and effector functional signatures in the same tumour tissues in patients with cancer.

In summary, we have shown that tumour cells metabolically and epigenetically impair T cell function and tumour immunity by outcompeting T cells for methionine via SLC43A2 (Extended Data Fig. 6). Our work demonstrates a long-suspected crosstalk between metabolism, histone pattern, and functional profile in tumour-infiltrating T cells. On this basis, selectively targeting tumour methionine metabolism may be a useful approach for cancer immunotherapy.

Online content

Any methods, additional references, Nature Research reporting summaries, source data, extended data, supplementary information, acknowledgements, peer review information; details of author contributions and competing interests; and statements of data and code availability are available at https://doi.org/10.1038/s41586-020-2682-1.

1. Wherry, E. J. T cell exhaustion. *Nat. Immunol.* **12**, 492–499 (2011).
2. Pauken, K. E. et al. Epigenetic stability of exhausted T cells limits durability of reinvigoration by PD-1 blockade. *Science* **354**, 1160–1165 (2016).
3. Sen, D. R. et al. The epigenetic landscape of T cell exhaustion. *Science* **354**, 1165–1169 (2016).
4. Philip, M. et al. Chromatin states define tumour-specific T cell dysfunction and reprogramming. *Nature* **545**, 452–456 (2017).
5. Zou, W., Wolchok, J. D. & Chen, L. PD-L1 (B7-H1) and PD-1 pathway blockade for cancer therapy: mechanisms, response biomarkers, and combinations. *Sci. Transl. Med.* **8**, 328rv4 (2016).
6. Horton, B. L., Williams, J. B., Cabanov, A., Spranger, S. & Gajewski, T. F. Intratumoral $CD8^+$ T-cell apoptosis is a major component of T-cell dysfunction and impedes antitumor immunity. *Cancer Immunol. Res.* **6**, 14–24 (2018).
7. Schoenborn, J. R. et al. Comprehensive epigenetic profiling identifies multiple distal regulatory elements directing transcription of the gene encoding interferon-γ. *Nat. Immunol.* **8**, 732–742 (2007).
8. Khan, O. et al. TOX transcriptionally and epigenetically programs $CD8^+$ T cell exhaustion. *Nature* **571**, 211–218 (2019).
9. Zhao, E. et al. Cancer mediates effector T cell dysfunction by targeting microRNAs and EZH2 via glycolysis restriction. *Nat. Immunol.* **17**, 95–103 (2016).
10. Song, M. et al. IRE1α-XBP1 controls T cell function in ovarian cancer by regulating mitochondrial activity. *Nature* **562**, 423–428 (2018).
11. Li, W. et al. Aerobic glycolysis controls myeloid-derived suppressor cells and tumor immunity via a specific CEBPB isoform in triple-negative breast cancer. *Cell Metab.* **28**, 87–103.e6 (2018).
12. Maj, T. et al. Oxidative stress controls regulatory T cell apoptosis and suppressor activity and PD-L1-blockade resistance in tumor. *Nat. Immunol.* **18**, 1332–1341 (2017).
13. Levine, A. J. & Puzio-Kuter, A. M. The control of the metabolic switch in cancers by oncogenes and tumor suppressor genes. *Science* **330**, 1340–1344 (2010).
14. Cairns, R. A., Harris, I. S. & Mak, T. W. Regulation of cancer cell metabolism. *Nat. Rev. Cancer* **11**, 85–95 (2011).
15. Guttormsen, A. B., Solheim, E. & Refsum, H. Variation in plasma cystathionine and its relation to changes in plasma concentrations of homocysteine and methionine in healthy subjects during a 24-h observation period. *Am. J. Clin. Nutr.* **79**, 76–79 (2004).
16. Schmidt, J. A. et al. Plasma concentrations and intakes of amino acids in male meat-eaters, fish-eaters, vegetarians and vegans: a cross-sectional analysis in the EPIC-Oxford cohort. Eur. *J. Clin. Nutr.* **70**, 306–312 (2016).
17. Qiu, J. et al. Acetate promotes T cell effector function during glucose restriction. *Cell Rep.* **27**, 2063–2074.e5 (2019).
18. Mentch, S. J. et al. Histone methylation dynamics and gene regulation occur through the sensing of one-carbon metabolism. *Cell Metab.* **22**, 861–873 (2015).
19. Shiraki, N. et al. Methionine metabolism regulates maintenance and differentiation of human pluripotent stem cells. *Cell Metab.* **19**, 780–794 (2014).
20. Min, J., Feng, Q., Li, Z., Zhang, Y. & Xu, R.-M. Structure of the catalytic domain of human DOT1L, a non-SET domain nucleosomal histone methyltransferase. *Cell* **112**, 711–723 (2003).
21. Nguyen, A. T. & Zhang, Y. The diverse functions of Dot1 and H3K79 methylation. *Genes Dev.* **25**, 1345–1358 (2011).
22. Jo, S. Y., Granowicz, E. M., Maillard, I., Thomas, D. & Hess, J. L. Requirement for Dot1l in murine postnatal hematopoiesis and leukemogenesis by MLL translocation. *Blood* **117**, 4759–4768 (2011).
23. Villarino, A., Kanno, Y. & O'Shea, J. Mechanisms and consequences of Jak–STAT signaling in the immune system. *Nat. Immunol.* **18**, 374–384 (2017).
24. Kagoya, Y. et al. DOT1L inhibition attenuates graft-versus-host disease by allogeneic T cells in adoptive immunotherapy models. *Nat. Commun.* **9**, 1915 (2018).
25. Schübeler, D. et al. The histone modification pattern of active genes revealed through genome-wide chromatin analysis of a higher eukaryote. *Genes Dev.* **18**, 1263–1271 (2004).
26. Barski, A. et al. High-resolution profiling of histone methylations in the human genome. *Cell* **129**, 823–837 (2007).
27. Kent, W. J. et al. The human genome browser at UCSC. *Genome Res.* **12**, 996–1006 (2002).
28. Rosenbloom, K. R. et al. ENCODE data in the UCSC Genome Browser: year 5 update. *Nucleic Acids Res.* **41**, D56–D63 (2013).
29. Alexander, S. P. H. et al. The concise guide to pharmacology 2019/20: transporters. *Br. J. Pharmacol.* **176** (Suppl. 1), S397–S493 (2019).
30. Tirosh, I. et al. Dissecting the multicellular ecosystem of metastatic melanoma by single-cell RNA-seq. *Science* **352**, 189–196 (2016).
31. Ma, E. H. et al. Serine is an essential metabolite for effector T cell expansion. *Cell Metab.* **25**, 345–357 (2017).
32. Geiger, R. et al. l-Arginine modulates T cell metabolism and enhances survival and anti-tumor activity. *Cell* **167**, 829–842.e13 (2016).
33. Roy, D. G. et al. Methionine metabolism shapes T helper cell responses through regulation of epigenetic reprogramming. *Cell Metab.* **31**, 250–266.e9 (2020).
34. Richon, V. M. et al. Chemogenetic analysis of human protein methyltransferases. *Chem. Biol. Drug Des.* **78**, 199–210 (2011).
35. Cavuoto, P. & Fenech, M. F. A review of methionine dependency and the role of methionine restriction in cancer growth control and life-span extension. *Cancer Treat. Rev.* **38**, 726–736 (2012).
36. Gao, X. et al. Dietary methionine influences therapy in mouse cancer models and alters human metabolism. *Nature* **572**, 397–401 (2019).

Methods

Mice

Six- to eight-week-old female wild-type C57BL/6, BALB/c, and *Rag1* knockout (KO) mice were obtained from the Jackson Laboratory. *Dot1l*$^{flox/flox}$ mice were bred with CD4-Cre mice to generate mice with specific *Dot1l* deletion in T cells. All *Dot1l*$^{+/+}$ or *Dot1l*$^{-/-}$ mice were used at the age of 6–12 weeks unless specified in the text. Mice were housed under specific pathogen-free conditions and handled according to the guidelines of the University Committee on the Use and Care of Animals at the University of Michigan.

Clinical studies

Patients with colorectal cancer were recruited for the methionine supplementation study. Eligible patients were of Eastern Cooperative Oncology Group performance status 0/1 with adequate organ and bone marrow function. Patients were excluded from this study if they had received or were receiving any concurrent chemotherapy, immunotherapy, biologic, and/or hormonal therapy for cancer. All patients took two capsules of methionine (500 mg per capsule, NOW Foods) daily for two weeks. This study was conducted according to the Declaration of Helsinki and approved by the institutional review board (IRB) of the Medical University of Lublin, with written informed consent obtained from all patients. Study participants were not compensated.

Human specimens

Plasma, peripheral blood mononuclear cells (PBMCs), and tumour-infiltrating T cells were isolated from healthy donors and patients with cancer. Plasma from patients diagnosed with high-grade serous ovarian carcinomas were collected for this study. Human specimens were collected with informed consent and procedures approved by the IRB of the University of Michigan.

Reagents

Amino acids, including L-isoleucine, L-leucine, L-lysine, L-methionine, L-phenylalanine, L-threonine, L-tryptophan, L-valine, L-histidine, L-arginine, L-cystine, L-tyrosine, and MEM non-essential amino acid solution (100×, including L-alanine, L-aspartic acid, L-asparagine, L-glutamic acid, L-glycine, L-proline and L-serine) were from Sigma. L-Glutamine (100×), 2-mercaptoethanol and dialysed fetal bovine serum (FBS) were from GIBCO. RPMI 1640 medium without amino acids and sodium phosphate powder (#R8999-04A) were from US Biological. 1× RPMI without L-glutamine, L-cysteine, L-cystine, and L-methionine was from MP Biomedicals. Methionine assay kit (Fluorometric) was from Abcam (ab234041). Anti-mouse CD3 and anti-CD28, anti-human CD3 and anti-CD28 monoclonal antibodies (mAbs) were from eBioscience. Mouse and human interleukin 2 (IL-2) were from R&D Systems, Inc.. *S*-(5-adenosyl)- L-methionine iodide (SAM), *S*-(5-adenosyl)- L-homocysteine (SAH), and L-cystathionine, as well as SLC transporter inhibitors, including α-(methylamino) isobutyric acid (MeAIB) and 2-amino-2-norbornanecarboxylic acid (BCH) were from Sigma. The DOT1L inhibitor EPZ004777 (#1338466-77-5) was from Millipore. Anti-mouse PD-L1 (clone: 10F.9G2) and rat IgG2B isotype (clone: LTF-2) were from Bioxcell.

Cell separation and culture

Human cells (including A375, CHL-1, SK-MEL-2 and 293T cells) and mouse tumour cells (including B16F10 and CT26 cells) were obtained from the ATCC. Mouse ID8-luc and MC38 cells were as previously reported[37,38]. Human primary high-grade serous ovarian carcinoma cells (OC8) were generated in our laboratory[38]. All cell lines in our laboratory are routinely tested for mycoplasma contamination and cells used in this study were negative for mycoplasma. None of our cell lines are on the list of commonly misidentified cell lines (International Cell Line Authentication Committee). Tumour cells were maintained in RPMI1640 (HyClone SH30255, GE Healthcare, Chicago, IL, USA) containing 10% (v/v) FBS (Alkali Scientific) and 1% (v/v) pen/strep (GIBCO).

Mouse lymphocytes were isolated from spleen and lymph nodes. CD8$^+$ T cells were separated using the EasySep Mouse CD8$^+$ T Cell Isolation Kit (STEMCELL Technologies Inc.). Human PBMCs were isolated from blood using Lymphoprep (STEMCELL Technologies Inc.). Human CD8$^+$ T cells were separated using the EasySep Human CD8$^+$ T Cell Isolation Kit (STEMCELL Technologies Inc.). CD8$^+$ T cells were re-suspended (10^6 cells/ml) and activated with anti-CD3 and anti-CD28 mAbs for 48 h. Activated CD8$^+$ T cells were maintained with IL-2 (10 ng/ml) and 2-mercaptoethanol, and cultured with fresh complete medium, media with or without individual amino acids, or tumour supernatants for 36–48 h. Media with or without amino acids were formulated with RPMI1640 (US Biological, #R8999-04A) by supplementation or omission of individual amino acids. The tumour supernatants were collected from medium initially cultured with tumour cells in RPMI lacking L-glutamine, L-cysteine, L-cystine, and L-methionine (MP Biomedicals #1646454), and subsequently supplemented with L-glutamine (GIBCO), L-cystine 2HCl (Sigma), and different concentrations of L-methionine (Sigma), as specified in different experiments. The following amino acids were used to supplement tumour culture supernatants: Iso 380 μM/l, Leu 380 μM/l, Lys 220 μM/l, Met 30 μM/l, Phe 90 μM/l, Thr 170 μM/l, Trp 20 μM/l, Val 170 μM/l, His 100 μM/l, Arg 1,160 μM/l, Cys 200 μM/l, Gln 2,000 μM/l, Tyr 110 μM/l, and other amino acids (MEM Non-essential Amino Acid Solution 100×, a mix of Ala, Asp, Asn, Glu, Gly, Pro, and Ser (Sigma)). The following metabolites were used to supplement tumour culture supernatants: Met 30 μM/l, SAM 50 μM/l, SAH 50 μM/l or L-cystathionine 100 μM/l.

Intratumour CD8$^+$ T cells from mice and humans were isolated as follows: mononuclear cells from the whole tumour or ascites suspension were first enriched by density gradient centrifugation using Lymphoprep (STEMCELL). CD8$^+$ T cells were further separated by a negative–positive two-step isolation. First, the enriched cells were isolated using the EasySep Mouse/Human CD8$^+$ T Cell Isolation Kit (negative selection, STEMCELL), then further enriched using the EasySep Mouse/Human CD8 Positive Selection Kit II (positive selection, STEMCELL). The purity of CD8$^+$ T cells was further determined by FACS staining.

Generation of knockdown cells

SLC43A2 knockdown cells were generated using the MISSION shRNA (Sigma) and GIPZ Lentiviral shRNA systems (Dharmacon, Inc.). 293T cells were co-transfected with lentiviral shRNA system together with plasmids psPAX2 and pMD2.G using Lipofectamine 2000 (Thermo Fisher Scientific) for lentivirus package. Forty-eight hours after transfection, the supernatant was collected. Tumour cells were infected with the virus supernatant for 24 h and then selected with 2 μg/ml puromycin (Santa Cruz Biotechnology) for an additional 48 h. Knockdown efficiency was validated by immunoblotting.

Flow cytometry analysis (FACS)

For FACS staining, cells were stained with a combination of fluorescence-conjugated mAbs from BD Biosciences or Thermo Fisher Scientific (Waltham). Mouse samples were stained with FITC-Annexin V, 7-AAD, PE-texas red-anti mouse CD45 (30-F11), FITC-anti-mouse CD90 (53-2.1), APC-Cy7-anti-mouse CD4 (RM4-5), AF700-anti-mouse CD8 (53-6.7), APC-anti-mouse IL-2 (JES6-5H4), BV786-anti-mouse IFNγ (XMG1.2), PE-Cy7-anti-mouse TNFα (MP6-XT22) and PE-anti-mouse granzyme B (NGZB) mAbs. Human samples were stained with FITC-Annexin V, 7-AAD, pacific blue-anti-human IFNγ (4S.B3), and APC-anti-human TNFα (MAb11). For apoptosis staining, cells were washed with 1× binding buffer (BD Biosciences) and stained with Annexin V and 7-AAD in 1× binding buffer in the dark for 10 min. For surface staining, the cells were incubated in the dark with antibodies for 30 min. For intracellular staining, the cells were fixed in Fix/Perm solution (BD Biosciences). After being washed with Perm/Wash buffer

(BD Biosciences), the cells were stained intracellularly for 30 min in the dark. For STAT5, cells were stained with APC-anti-STAT5 (REA549, Miltenyi Biotec Inc.). For DOT1L and H3K79me2 intracellular staining, the cells were first stained with DOT1L or H3K79me2 antibodies (Abcam), and then stained using a FITC-conjugated goat anti-rabbit IgG (H + L) secondary antibody (Invitrogen). All samples were acquired on BD LSRFortessa (BD Biosciences) and were analysed using FACSDiva (BD Biosciences) or FlowJo (FlowJo LLC).

Chromatin immunoprecipitation

ChIP assay was performed according to the manufacturer's protocol (Millipore). In brief, crosslinking was performed with 1% formaldehyde or 1% paraformaldehyde for 10 min. To enhance cell lysis, we ran the lysate through a 27-g needle three times and flash froze it at −80 °C. Sonication was then performed using the the Misonix 4000 water bath sonication unit at 15% amplitude for 20 min. Protein–DNA complex was precipitated by specific antibodies against H3K79me2 (Abcam) and IgG control (Millipore). DNA was purified using DNA Purification Kit (Qiagen). ChIP-enriched chromatin was used for real-time PCR. Relative expression levels were normalized to Input. Specific primers are listed in Extended Data Table 1.

Real-time PCR and western blotting

$CD8^+$ T cells were incubated in fresh medium or specific tumour supernatant for 24–48 h. Tumour cells were maintained with complete medium. The cells were washed and collected. RNA was isolated from these cells using Direct-zolTM RNA miniprep Plus kit (ZOMO research), and then subjected to reverse transcription using first-strand cDNA Synthesis for Quantitative RT–PCR kit (OriGene). Real-time PCR was performed using SYBR green chemistry (Applied Biosystems). Reactions were run on a real-time PCR system (StepOnePlus Real-Time PCR System, Applied Biosystem). Specific primers are listed in Extended Data Table 3.

For western blotting, $CD8^+$ T and tumour cells were washed and lysed in a modified RIPA buffer with 1× protease inhibitor cocktail (Roche). The lysates were stored at −80 °C until immunoblot analysis. For histone isolation, $CD8^+$ T cells were first lysed with PBS with 0.5% Triton X-100. The lysates were then incubated on ice for 10 min and cleared by centrifugation at 5,000*g* for 15 min. The precipitate was dissolved with 0.2 N HCl. Protein concentration was quantified using a BCA protein assay kit (Thermo Fisher Scientific) and denatured at 95 °C for 5 min. The lysate samples were stored at −80 °C for immunoblot analysis. In brief, the proteins were separated electrophoretically using a 12% SDS-polyacrylamide gel and transferred onto an PVDF membrane (Millipore). The membranes were blocked in 5% fat-free milk for 1 h, and then incubated with a specific primary antibody at 4 °C overnight. Blots were probed with rabbit anti-H3K79me2, H3K4me2, H3K4me3, H3K9me2, H3K27me2, total H3, STAT5, p-STAT5, STAT1, STAT3, SLC43A2, SLC7A5 and β-actin antibodies. All antibodies were from Abcam or Cell Signaling Technology. After hybridization with HRP-conjugated secondary antibody (Life Technologies), protein bands were visualized using a chemiluminescence detection kit (Bio-Rad Laboratories).

Tumour inoculation and treatments

For the in vivo tumour growth experiments, mice were inoculated subcutaneously with 2×10^5 B16F10 cells or 5×10^5 MC38 cells, or intraperitoneally with 2×10^6 ID8-Luc ovarian cancer cells. The B16F10 and MC38 tumour volumes were measured along three orthogonal axes (*a*, *b*, and *c*) and were calculated as follows: tumour volume = $a \times b \times c/2$. The ID8-luc tumour growth was monitored using the Xenogen IVIS Spectrum In vivo Bioluminescence Imaging System (PerkinElmer). Tumour load was calculated based on the total flux (photons per second). Anti-PD-L1 and IgG1 isotype mAbs (Bioxcell) were given intraperitoneally at a dose of 100 μg per mouse on day 7 after tumour cell inoculation, then every 3 days for the duration of the experiment. 2-Amino-2-norbornanecarboxylic acid (BCH) was given intravenously at a dose of 180 mg/kg per mouse on day 7 after tumour inoculation, then every 2 days for the duration of the experiment. Methionine was given by intratumour (B16F10 model) or intraperitoneal (ID8 model) injection at a dose of 40 mg/kg per mouse on day 7 after tumour inoculation, then every 2 days for the duration of the experiment. Animal studies were conducted under the approval of the University of Michigan Committee on Use and Care of Animals. In none of the experiments did tumour size surpass 2 cm in any dimension. No mouse had severe abdominal distension (≥10% original body weight increase). Sample size was chosen on the basis of preliminary data. After tumour inoculation, mice were randomized and assigned to different groups for treatment.

RNA-seq and bioinformatics analysis

$CD8^+$ T cells were cultured in complete fresh medium, tumour supernatant (sup), or tumour supernatant plus methionine (sup + met) for 24 h. $CD8^+$ T cells from *Dot1l*$^{-/-}$ mice and littermates (*Dot1l*$^{+/+}$) were isolated and sorted. The RNA was isolated by using Direct-zolTM RNA miniprep Plus kit (ZOMO research). RNA-seq and RNA-array were conducted in $CD8^+$ T cells by the DNA sequencing core at the University of Michigan. The data were processed by the Bioinformatic Core at the University of Michigan, and analysed with ClueGo[39] and GSEA software v. 3.0[40]. RNA sequencing data that support the findings of this study have been deposited in NCBI Gene Expression Omnibus (GEO) under accession number GSE150887. Public RNA-seq data were from GSE108694 and GSE72056. For single cell RNA-seq data in patients with melanoma, the expression levels of genes were quantified as $E_{i,j} = \log_2(\mathrm{TPM}_{i,j}/10 + 1)$, where $\mathrm{TPM}_{i,j}$ refers to transcripts per million (TPM) for gene *i* in sample *j*[30]. We then evaluated the average $E_{i,j}$ values of tumour cell *SLC43A2* transcripts[41–43]. Based on the median of average $E_{i,j}$ values, we divided the patients into high (average SLC43A2 $E_{i,j} > 0.056$, including patients 53, 79, 81, 82, 84, and 94) and low (average SLC43A2 $E_{i,j} < 0.056$, including patients 60, 65, 71, 80, 88, and 89) groups. GSEA analysis for tumour-infiltrating T cells was characterized and compared between patients with high and low levels of *SLC43A2* expression.

Metabolomics

Metabolomics and sample collection were performed as previously reported[44,45]. In brief, $CD8^+$ T cells were collected and transferred to a 15-ml tube for centrifugation at 300*g* for 5 min at 4 °C. Cells were then washed with cold PBS. After further centrifugation at 300*g* for 5 min at 4 °C, 1 ml of 80% cold methanol was added and vigorously vortexed to ensure the cell pellet was completely disrupted. The samples were placed on dry ice and moved to a −80 °C freezer for 10 min, followed by vigorous vortexing. The samples were again centrifuged at maximum speed for 10 min at 4 °C. The supernatant was collected in new tubes and normalized by protein concentration. Samples were kept at −80 °C until analysis. We used liquid chromatography–mass spectrometry to detect intracellular metabolites in $CD8^+$ T cells and amino acids in human serum from healthy donors and patients with ovarian cancer. Intracellular SAM and amino acids in B16F10 supernatants were measured in Creative-proteomics.

Statistical analysis

Statistical analysis was performed using GraphPad Prism statistical software (version 7, GraphPad Software Inc.). Error bars in data represent s.e.m. Inter-group data were analysed using an unpaired or paired two-tailed *t*-test. Tumour growth was analysed using two-way ANOVA. Survival functions were estimated using the Kaplan–Meier method. A log-rank test was used to calculate the statistical differences. The correlations between tumour *SLC43A2* and immune-associated genes were analysed using Pearson's correlation test. A value of $P < 0.05$ was considered statistically significant. Experiments were not randomized unless otherwise stated, and experimenters were not blinded to allocation during experiments and outcome assessment.

Statistics and reproducibility

Figure 1a–d, $n = 3$ biologically independent samples. The experiments were performed three times with similar results. a, $^{****}P < 0.0001$ compared with complete medium (CM) by two-tailed unpaired *t*-test; b, $^{***}P = 0.001$ compared with CM by two-tailed unpaired *t*-test; c, $^{****}P < 0.0001$ compared with CM by two-tailed unpaired *t*-test, d, $^{****}P < 0.0001$ by two-tailed unpaired *t*-test. e, $n = 4$ biologically independent samples. The experiments were performed three times with similar results. $^{**}P = 0.0014$, $^{****}P < 0.0001$ by two-tailed unpaired *t*-test. f, $n = 3$ biologically independent samples. The experiments were performed once. g–j, $n = 3$ biologically independent samples. The experiments were performed three times with similar results. g, $^{****}P < 0.0001$ compared with supernatant (sup) by two-tailed unpaired *t*-test. h, $^{***}P = 0.0002$, $^{****}P < 0.0001$ compared with sup by two-tailed unpaired *t*-test. i, NS $P = 0.6597$, $^{***}P = 0.0007$, and $^{***}P = 0.0002$ by two-tailed unpaired *t*-test. k, l, $n = 4$ biologically independent samples. The experiments were performed three times with similar results.

Figure 2a, b, $n = 4$ biologically independent samples. $CD8^+$ T cells were cultured with fresh medium (FM), B16F10 tumour supernatants (sup) and B16F10 supernatants with methionine supplementation (sup + met). GSEA plot showed enriched apoptotic and defective TCR signaling pathways (a), as well as defective methionine metabolism signalling (b) in T cells cultured in tumour supernatant. c–f, $n = 4$ biologically independent samples. The experiments were performed three times with similar results. d, $^{***}P = 0.0006$ FM vs sup, and $^{***}P = 0.0005$ sup vs sup + met by two-tailed unpaired *t*-test. e, $^{****}P < 0.0001$ FM vs sup, and $^{*}P = 0.0183$ sup vs sup + met by two-tailed unpaired *t*-test. f, $^{****}P < 0.0001$ FM vs sup, and $^{**}P = 0.0082$ sup vs sup + met by two-tailed unpaired *t*-test. g, h, $n = 3$ biologically independent samples. The experiments were performed three times with similar results. $^{****}P < 0.0001$ by two-tailed unpaired *t*-test. i, j, The experiments were performed three times with similar results.

Figure 3a, The experiments were performed three times with similar results. b, c, $n = 4$ biologically independent samples. The experiments were performed three times with similar results. b, $^{****}P < 0.0001$ by two-tailed unpaired *t*-test. c, $^{****}P < 0.0001$, $^{*}P = 0.0497$, $^{**}P = 0.0025$ by two-tailed unpaired *t*-test. d, The experiments were performed three times with similar results. e, $n = 6$ biologically independent samples in fresh $CD8^+$, and $n = 8$ biologically independent samples in activated $CD8^+$. The experiments were performed twice with similar results. $^{***}P = 0.0001$, $^{****}P < 0.0001$ by two-tailed unpaired *t*-test. f, $n = 4$ biologically independent samples. The experiments were performed three times with similar results. $^{*}P = 0.0165$ by two-tailed unpaired *t*-test. g–i, $n = 4$ biologically independent samples. The experiments were performed twice with similar results. g, $^{*}P = 0.0109$ by two-tailed unpaired *t*-test. h, Day 19 $^{*}P = 0.0169$, Day 22 and Day 25 $^{****}P < 0.0001$ by two-way ANOVA. i, $^{*}P = 0.014$, $^{***}P = 0.0008$ by two-tailed unpaired *t*-test. j, k, $n = 4$ biologically independent samples. The experiments were performed twice with similar results. $^{****}P < 0.0001$ by two-tailed unpaired *t*-test. l, m, $n = 3$ biologically independent samples. The data were from RNA array of *Dot1l*$^{+/+}$ and *Dot1l*$^{-/-}$ $CD8^+$ T cells. n, o, The experiments were performed three times with similar results. p, q, $n = 3$ biologically independent samples. The experiments were performed three times with similar results. q, Site1: $^{***}P = 0.0002$ sup vs sup + met, $^{****}P < 0.0001$ sup vs FM by two-tailed unpaired *t*-test. Site2: $^{***}P = 0.0002$ sup vs FM, $^{***}P = 0.0001$ sup vs sup + met by two-tailed unpaired *t*-test.

Figure 4a, $n = 10$ biologically independent animals. The experiments were performed once. Day 17 $^{*}P = 0.0291$ by two-tailed unpaired two-way ANOVA. b, $n = 7$ biologically independent animals. $^{*}P = 0.0114$ by two-tailed unpaired *t*-test. c, $n = 6$ biologically independent animals. $^{*}P = 0.0292$ by two-tailed unpaired *t*-test. d, $n = 6$ biologically independent animals. $^{*}P = 0.0395$ by two-tailed unpaired *t*-test. e, $n = 8$ biologically independent animals. IL-2: $^{*}P = 0.0106$ by two-tailed unpaired *t*-test. TNFα: $^{*}P = 0.0131$ by two-tailed unpaired *t*-test. IFNγ: $^{**}P = 0.0027$ by two-tailed unpaired *t*-test. f, $n = 20$ biologically independent animals. The experiments were performed once. Day 41 $^{*}P = 0.0046$ by two-tailed unpaired two-way ANOVA. g, $n = 14$ biologically independent animals. IL-2: $^{*}P = 0.0161$ by two-tailed unpaired *t*-test. TNFα: $^{**}P = 0.0046$ by two-tailed unpaired *t*-test. IFNγ: $^{**}P = 0.0024$ by two-tailed unpaired *t*-test. h, $n = 6$ biologically independent samples. IL-2: $^{***}P = 0.0004$ by two-tailed unpaired *t*-test. TNFα: $^{****}P < 0.0001$ by two-tailed unpaired *t*-test. IFNγ: $^{*}P = 0.0328$ by two-tailed unpaired *t*-test. i–l, $n = 7$ patients with colorectal cancer received methionine supplementation. i, j, Representative results were shown from four patients. k, l, TNFα: $^{*}P = 0.0181$ by two-tailed paired *t*-test. IFNγ: $^{*}P = 0.0404$ by two-tailed paired *t*-test. Annexin V: $^{*}P = 0.0497$ by two-tailed paired *t*-test.

Figure 5a–d, $n = 3$ biologically independent animals. The experiments were performed three times with similar results. a, $^{***}P = 0.0001$, $^{****}P < 0.0001$ by two-tailed unpaired *t*-test. b-d, $^{****}P < 0.0001$ by two-tailed unpaired *t*-test. e, The experiments were performed three times with similar results. f, $n = 8$ biologically independent animals. The experiments were performed twice with similar results. Day 27 $^{***}P = 0.0006$ by two-tailed unpaired two-way ANOVA. g, $n = 6$ biologically independent animals. The experiments were performed twice with similar results. TNFα: $^{*}P = 0.0494$ by two-tailed unpaired *t*-test. IFNγ: $^{**}P = 0.0496$ by two-tailed unpaired *t*-test. Granzyme B: $^{*}P = 0.0434$ by two-tailed unpaired *t*-test. h, $n = 18$ biologically independent animals. The experiments were performed twice with similar results. Day 22 $^{**}P = 0.0023$ anti-PD-L1 + BCH vs anti-PD-L1, $^{****}P < 0.0001$ anti-PD-L1 + BCH vs PBS + IgG or BCH by two-tailed unpaired two-way ANOVA. i, $n = 5$ in PBS + IgG, $n = 9$ in other groups biologically independent animals. The experiments were performed twice with similar results. TNFα: $^{*}P = 0.0263$ anti-PD-L1 + BCH vs anti-PD-L1, $^{**}P = 0.0082$ anti-PD-L1 + BCH vs PBS + IgG by two-tailed unpaired *t*-test. IFNγ: $^{**}P = 0.0046$ anti-PD-L1 + BCH vs PBS + IgG, $^{**}P = 0.0013$ anti-PD-L1 + BCH vs BCH, $^{**}P = 0.0086$ anti-PD-L1 + BCH vs anti-PD-L1 by two-tailed unpaired *t*-test. Granzyme B: $^{*}P = 0.0235$ anti-PD-L1 + BCH vs PBS + IgG, $^{**}P = 0.0426$ anti-PD-L1 + BCH vs BCH, $^{**}P = 0.0484$ anti-PD-L1 + BCH vs anti-PD-L1 by two-tailed unpaired *t*-test. j, k, $n = 9$ biologically independent animals. The experiments were performed twice with similar results. Day 33 $^{*}P = 0.0167$ anti-PD-L1 + BCH vs anti-PD-L1, $^{**}P = 0.0038$ anti-PD-L1 + BCH vs BCH, $^{****}P < 0.0001$ anti-PD-L1 + BCH vs PBS + IgG by two-tailed unpaired two-way ANOVA. l, $n = 5$ in PBS + IgG, $n = 7$ in other groups biologically independent animals. The experiments were performed twice with similar results. TNFα: $^{*}P = 0.0478$ anti-PD-L1 + BCH vs PBS + IgG, $^{*}P = 0.0498$ anti-PD-L1 + BCH vs BCH, $^{*}P = 0.0425$ anti-PD-L1 + BCH vs anti-PD-L1 by two-tailed unpaired *t*-test. IFNγ: $^{*}P = 0.0269$ anti-PD-L1 + BCH vs PBS + IgG, $^{**}P = 0.0013$ anti-PD-L1 + BCH vs BCH, $^{**}P = 0.0331$ anti-PD-L1 + BCH vs anti-PD-L1 by two-tailed unpaired *t*-test. m, RNA-seq analysis showed expression of SLC43A2 transcripts in tumours and paired adjacent normal tissues in several types of tumour. CHOL, $n = 9$, $^{**}P = 0.0013$; ESCA, $n = 11$, $^{**}P = 0.0070$; HNSC, $n = 43$, $^{**}P = 0.0016$; KICH, $n = 24$, $^{****}P < 0.0001$; LIHC, $n = 50$, $^{*}P = 0.0273$ by two-tailed paired *t*-test.

Extended Data Figure 1a–c, $n = 4$ biologically independent samples. The experiments were performed three times with similar results. a, $^{****}P < 0.0001$ by two-tailed unpaired *t*-test. b, $^{***}P = 0.0002$ 100 μM vs FM, $^{***}P = 0.0005$ 50 μM vs FM, $^{***}P = 0.0019$ 30 μM vs FM by two-tailed unpaired *t*-test. c, $^{*}P = 0.0372$, $^{****}P < 0.0001$ by two-tailed unpaired *t*-test. d, e, $n = 4$ biologically independent samples. The experiments were performed twice with similar results. d, $^{*}P = 0.038$ sup vs FM, $^{*}P = 0.0139$ sup vs sup + met by two-tailed unpaired *t*-test. e, TNFα: $^{***}P = 0.0003$ sup vs FM, $^{****}P < 0.0001$ sup vs sup + met by two-tailed unpaired *t*-test. IFNγ: $^{****}P < 0.0001$ svs FM, $^{***}P = 0.0003$ sup vs sup + met by two-tailed unpaired *t*-test. f, g, $n = 11$ biologically independent donors in healthy control, and $n = 14$ biologically independent donors in patients with ovarian cancer. The experiments were performed once. g, $^{*}P = 0.0201$ by two-tailed unpaired *t*-test. h, $n = 3$ biologically

independent samples. The experiments were performed once. *P = 0.0531 by two-tailed unpaired t-test. i, n = 3 biologically independent samples. The experiments were performed twice with similar results. *P = 0.0306, **P = 0.0090 by two-tailed unpaired t-test. k–m, n = 5 biologically independent samples. The experiments were performed twice with similar results. ****P < 0.0001 by two-tailed unpaired t-test. o, p, n = 4 biologically independent animals. The experiments were performed twice with similar results. EC50 was determined by nonlinear regression (log (agonist) vs. response).

Extended Data Figure 2a–e, n = 4 biologically independent samples. RNA-seq in $CD8^+$ T cells. f, n = 4 biologically independent samples. The experiments were performed twice with similar results. h, i, n = 4 biologically independent samples. The experiments were performed twice with similar results. h, ****p sup vs FM, **P = 0.0097 sup vs sup + met by two-tailed unpaired t-test. i, **P = 0.0040 sup vs FM, **P = 0.0075 sup vs sup + met by two-tailed unpaired t-test. j, k, The experiments were performed three times with similar results.

Extended Data Figure 3a, b, The experiments were performed three times with similar results. c–e, n = 4 biologically independent samples. Gene signature comparison between *Dot1l*$^{-/-}$ and Dot1l$^{+/+}$ $CD8^+$ T cells through RNA array. f, n = 4 biologically independent samples. The experiments were performed twice with similar results. TNFα: *P = 0.0254 sup by two-tailed unpaired t-test. IFNγ: **P = 0.0032 by two-tailed unpaired t-test. Granzyme B: ***P = 0.0006 by two-tailed unpaired t-test. g, n = 5 biologically independent animals. The experiments were performed once. Day 16 *P = 0.0246 *Dot1l*$^{+/+}$ vs *Dot1l*$^{-/-}$, ****P < 0.0001 *Dot1l*$^{+/+}$ vs *Dot1l*$^{-/-}$ + anti-PD-L1, NS P = 0.9402 *Dot1l*$^{-/-}$ vs *Dot1l*$^{-/-}$ + anti-PD-L1 by two-tailed unpaired two-way ANOVA. h, n = 5 biologically independent samples. The experiments were performed twice with similar results. Day 14 **P = 0.003 by two-tailed unpaired two-way ANOVA. i, n = 4 biologically independent samples. The experiments were performed twice with similar results. *P = 0.0199 in dLN CD8, and *P = 0.0142 in tumour CD8 by two-tailed unpaired t-test. j, n = 4 biologically independent samples. The experiments were performed twice with similar results. Stat5a: *P = 0.0111 in fresh *Dot1l*$^{+/+}$ vs *Dot1l*$^{-/-}$ $CD8^+$ T cells, *P = 0.0144 in activated *Dot1l*$^{+/+}$ vs *Dot1l*$^{-/-}$ $CD8^+$ T cells. Stat5b: *P = 0.0116 in fresh *Dot1l*$^{+/+}$ vs *Dot1l*$^{-/-}$ $CD8^+$ T cells, ****P < 0.0001 in activated *Dot1l*$^{+/+}$ vs *Dot1l*$^{-/-}$ $CD8^+$ T cells. k, n = 3 biologically independent samples. The experiments were performed twice with similar results. Stat5b: *P = 0.0140 sup vs FM, **P = 0.0087 sup vs sup + met. l–n, n = 3 biologically independent samples. RNA-seq showed the effect of DOT1L inhibitor (SGC0946) on human $CD8^+$ T cells (PDB: GSE108694).

Extended Data Figure 4a, n = 6 biologically independent samples. **P = 0.0036 by two-tailed unpaired t-test. b, n = 6 biologically independent samples. **P = 0.0016 by two-tailed unpaired t-test. c, n = 5 biologically independent samples. ****P < 0.0001 by two-tailed unpaired t-test. d, n = 5 biologically independent samples. P = 0.0666 by two-tailed unpaired t-test. e, n = 6 biological independent clinical samples. The experiment was performed once. f, n = 6 biologically independent samples. *P = 0.0483 by two-tailed unpaired t-test. g, n = 6 biologically independent samples. **P = 0.0446 by two-tailed unpaired t-test. h, n = 5 biologically independent samples. **P = 0.0055 by two-tailed unpaired t-test. i, n = 5 biologically independent samples. P = 0.0596 by two-tailed unpaired t-test. j, n = 4 biologically independent samples. ****P < 0.0001 by two-tailed unpaired t-test. k, n = 4 biologically independent samples. ****P < 0.0001 by two-tailed unpaired t-test. l, n = 4 biologically independent samples. *P = 0.0155 by two-tailed unpaired t-test. m, n = 4 biologically independent samples. ****P < 0.0001 by two-tailed unpaired t-test. n, n = 5 biologically independent samples. NS P = 0.7891 in $CD45^-$ tumour, *P = 0.0217 in T cell by two-tailed unpaired t-test. o, n = 10 biologically independent samples. **P = 0.0045 by two-tailed unpaired t-test. p, n = 10 biologically independent animals. ****P < 0.0001 by two-tailed unpaired two-way ANOVA. q, n = 10 biologically independent samples. **P = 0.0011 met + anti-PD-L1 vs PBS + IgG, *P = 0.0219 met + anti-PD-L1 vs met + IgG, *P = 0.0492 met + anti-PD-L1 vs PBS + anti-PD-L1 by two-tailed unpaired t-test. r, n = 10 biologically independent samples. *P = 0.0220 met + anti-PD-L1 vs PBS + IgG, *P = 0.0444 met + anti-PD-L1 vs PBS + anti-PD-L1 by two-tailed unpaired t-test.

Extended Data Figure 5a, n = 3 biologically independent samples. The experiments were performed three times with similar results. **P = 0.0067, ****P < 0.0001 by two-tailed unpaired t-test. b, n = 3 biologically independent samples. The experiments were performed three times with similar results. ***P = 0.0002, ****P < 0.0001 by two-tailed unpaired t-test. c, n = 3 biologically independent samples. The experiments were performed twice with similar results. ****P < 0.0001 by two-tailed unpaired t-test. d, The experiments were performed twice with similar results. e, The experiments were performed three times with similar results. f, The experiments were performed twice with similar results. g, n = 3 biologically independent samples. The experiments were performed once. *P = 0.0277, **P = 0.0065 by two-tailed unpaired t-test. h, n = 5 biologically independent animals. The experiments were performed once. i, n = 7 biologically independent animals. The experiments were performed once. j, n = 5 biologically independent samples. The experiments were performed twice with similar results. *P = 0.0263 by two-tailed unpaired t-test. k, n = 8 biologically independent animals. The experiments were performed once. ****P < 0.0001 by two-tailed unpaired two-way ANOVA. l, The experiments were performed twice with similar results. m, n = 9 biologically independent animals. The experiments were performed once. n, n = 5 biologically independent animals. The experiments were performed twice with similar results. Day 35 *P = 0.0102 by two-tailed unpaired two-way ANOVA. o, n = 4 biologically independent samples. The experiments were performed twice with similar results. *P = 0.0415 in ID8 ascites, **P = 0.0389 in ID8 tumour by two-tailed unpaired t-test. p, n = 5 biologically independent samples. The experiments were performed twice with similar results. T cells: **P = 0.0029 BCH + anti-PD-L1 vs PBS + IgG, **P = 0.0094 BCH + anti-PD-L1 vs BCH, *P = 0.0461 BCH + anti-PD-L1 vs anti-PD-L1 by two-tailed unpaired t-test. CD8 cells: **P = 0.0049 BCH + anti-PD-L1 vs PBS + IgG, *P = 0.0136 BCH + anti-PD-L1 vs BCH, *P = 0.0480 BCH + anti-PD-L1 vs anti-PD-L1 by two-tailed unpaired t-test. q–s, Kaplan–Meier survival curves showed the relationship between levels of SLC43A2 and survival of patients with different types of tumour: cholangiocarcinoma (CHOL, p), low grade glioma (LGG, q), and lung squamous cell carcinoma (LUSC, r). The raw data were from TCGA. t–y, n = 12 independent patients. Single cell RNA-seq analyses were based on GSE72056. t, *P = 0.0485 by two-tailed paired t-test. v, Correlation was analysed using Pearson correlation analysis.

Reporting summary

Further information on research design is available in the Nature Research Reporting Summary linked to this paper.

Data availability

RNA sequencing data that support the findings of this study have been deposited in NCBI Gene Expression Omnibus (GEO) under accession number GSE150887. All other data that supported the findings of this study are available from the corresponding author upon request. Source data are provided with this paper.

37. Roby, K. F. et al. Development of a syngeneic mouse model for events related to ovarian cancer. *Carcinogenesis* **21**, 585–591 (2000).
38. Wang, W. et al. Effector T cells abrogate stroma-mediated chemoresistance in ovarian cancer. *Cell* **165**, 1092–1105 (2016).
39. Bindea, G. et al. ClueGO: a Cytoscape plug-in to decipher functionally grouped gene ontology and pathway annotation networks. *Bioinformatics* **25**, 1091–1093 (2009).
40. Subramanian, A. et al. Gene set enrichment analysis: a knowledge-based approach for interpreting genome-wide expression profiles. *Proc. Natl Acad. Sci. USA* **102**, 15545–15550 (2005).
41. Bacher, R. & Kendziorski, C. Design and computational analysis of single-cell RNA-sequencing experiments. *Genome Biol.* **17**, 63 (2016).

42. Wagner, G. P., Kin, K. & Lynch, V. J. Measurement of mRNA abundance using RNA-seq data: RPKM measure is inconsistent among samples. *Theor. den Biowissenschaften* **131**, 281–285 (2012).
43. Hwang, B., Lee, J. H. & Bang, D. Single-cell RNA sequencing technologies and bioinformatics pipelines. *Exp. Mol. Med*. **50**, 96 (2018).
44. Lee, H.-J., Kremer, D. M., Sajjakulnukit, P., Zhang, L. & Lyssiotis, C. A. A large-scale analysis of targeted metabolomics data from heterogeneous biological samples provides insights into metabolite dynamics. *Metabolomics* **15**, 103 (2019).
45. Yuan, M. et al. Ex vivo and in vivo stable isotope labelling of central carbon metabolism and related pathways with analysis by LC-MS/MS. *Nat. Protocols* **14**, 313–330 (2019).

Acknowledgements We thank P. King for scientific input. We acknowledge support from the Advanced Genomics Core and Bioinformatics Core of the University of Michigan Medical School's Biomedical Research Core Facilities. This work was supported in part by research grants from the US NIH/NCI (W. Zou) (CA217648, CA123088, CA099985, CA193136 and CA152470) and the NCI Cooperative Human Tissue Network (CHTN). C.A.L. was supported by a 2017 AACR NextGen Grant for Transformative Cancer Research (17-20-01-LYSS) and an ACS Research Scholar Grant (RSG-18-186-01). Metabolomics studies performed at the University of Michigan were supported by NIH grant DK097153, the Charles Woodson Research Fund, and the University of Michigan Pediatric Brain Tumor Initiative. C.A.L. and W. Zou were supported by the NIH through the University of Michigan Rogel Cancer Center Grant (P30 CA046592).

Author contributions Y.B., W.L., and W. Zou proposed the research concept. Y.B. performed the majority of the experiments and explored the concept for the SLC transporter. Y.B., W.L., and W. Zou designed the experiments. W.L. and J.C. performed some in vivo experiments with *Dot1l*$^{-/-}$ mice. D.M.K., P.S., L.Z., Z.C.N. and C.A.L. designed, performed, and analysed the MS experiments for metabolite tests and analysis. S.L., J.L., M.C. and A.M.C. assisted with the RNA-seq and single cell RNA-seq data analysis. H.X., P.L., J.Y., L.V., W.S., and I.K. aided in mouse and human sample collection and FACS data analysis. S.W. and S.G performed mouse genotyping and breeding. J.R.L. and K.M. assisted in clinical study design and collection of specimens from patient with ovarian cancer. A.C., A.P., W. Zgodziński, G.W., I.W., and K.O. performed the clinical study on patients with colorectal cancer. Y.B., W.L., and W. Zou wrote the manuscript.

Competing interests The authors declare no competing interests.

Additional information

Supplementary information is available for this paper at https://doi.org/10.1038/s41586-020-2682-1.

Correspondence and requests for materials should be addressed to W.Z.

Peer review information *Nature* thanks Tak Mak, Stefani Spranger and the other, anonymous, reviewer(s) for their contribution to the peer review of this work.

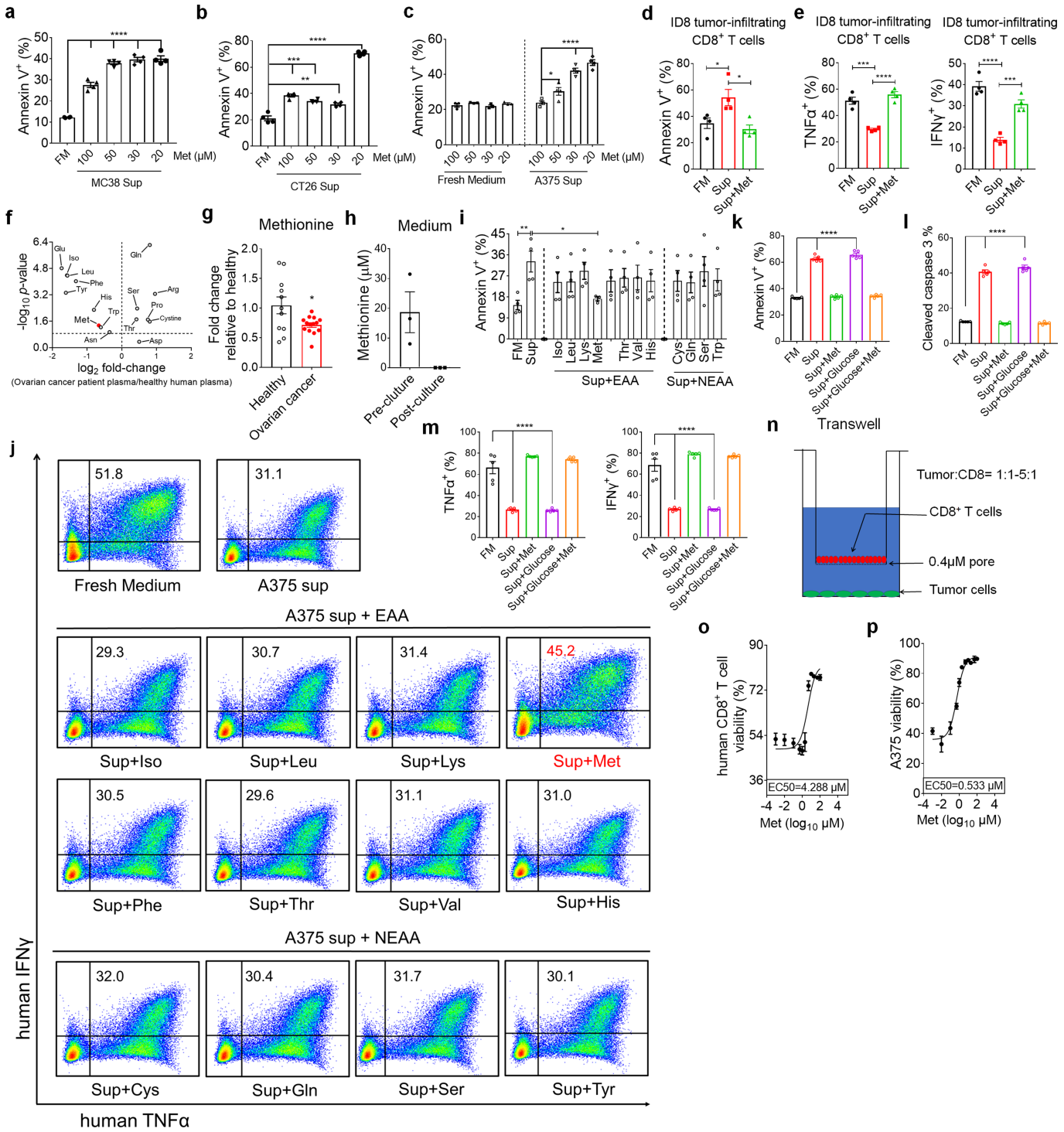

Extended Data Fig. 1 | Tumour cells outcompete T cells for methionine to impair T cell function. a–**c**, Effect of tumour cells on T cell apoptosis. Tumour supernatants were collected from MC38 (**a**), CT26 (**b**), and human melanoma A375 (**c**) tumour cells cultured for 48 h with media containing different concentrations of methionine (Met). Then, $CD8^+$ T cells were cultured for 36 h with these tumour supernatants (Sup) or fresh medium. Apoptosis was determined by Annexin V staining. **d**, **e**, Effect of methionine on ID8 tumour infiltrating cells. T cells were cultured with fresh medium, ID8 supernatant (Sup), and supernatant plus methionine (Sup + Met). T cell apoptosis (**d**) and cytokine production (**e**) were determined by FACS. **f**, **g**, Amino acid levels in ovarian cancer patient plasma. Amino acids were detected in healthy donor and ovarian cancer patient plasma by liquid chromatography mass spectrometry (LC-MS). (**f**) Volcano showed plasma free amino acid changes. Red dot showed methionine (Met). (**g**) Plasma methionine in ovarian cancer patients vs healthy controls. **h**, Methionine concentration in pre- and post- tumour cultured medium. **i**, **j**, Effect of amino acid supplementation on human T cell function. $CD8^+$ T cells were cultured with A375 supernatants (Sup) supplemented with different amino acids for 36 h. FACS analysis showed T cell apoptosis (**i**) and effector cytokines (**j**). **k**–**m**, Effect of glucose supplementation on the role of methionine-affected T cell apoptosis and function. **n**, Schematic figure showing tumour and T cell co-culture in the Transwell system. **o**, **p**, Effect of methionine on human $CD8^+$ T cell (**o**) and tumour cell (**p**) viability, EC_{50} was determined by nonlinear regression (log(agonist) vs. response). Sup, tumour supernatant. Data are mean ± s.e.m. Information on sample sizes, experimental number, times, biological replicates, statistical tests, and *P* values is available in 'Statistics and reproducibility' (Methods).

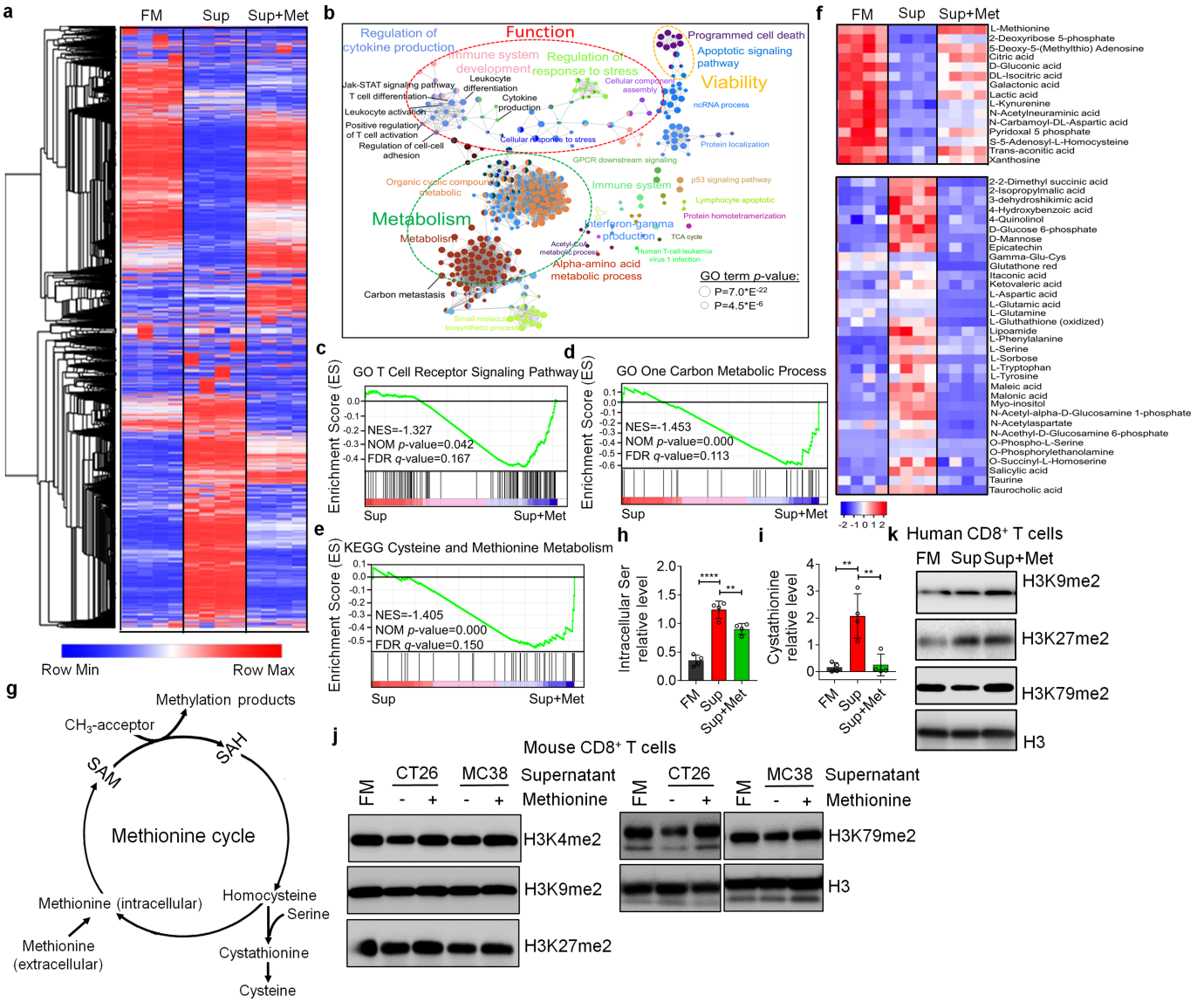

Extended Data Fig. 2 | Tumour alters CD8$^+$ T cell methionine metabolism to diminish H3K79me2. a, Gene profile changes in CD8$^+$ T cells. Mouse CD8$^+$ T cells were cultured with fresh medium, B16F10 tumour supernatant (Sup), or tumour supernatants plus methionine (Sup + Met) for 36 h. Gene profile changes were analysed by RNA-seq. **b**, Gene signatures were compared between groups from fresh medium and Sup. Functionally grouped network of enriched categories was generated for the hub genes and their regulators using ClueGO. Visualization has been carried out using Cytoscape 3.7.1. **c**–**e**, GSEA plot showed recovery of TCR signalling pathway (**c**) and methionine metabolism signalling (**d**, **e**) in CD8$^+$ T cells cultured with Sup + Met compared to Sup. **f**, Metabolites changes in CD8$^+$ T cells cultured with fresh medium, Sup and Sup + Met. Upper panel: Metabolites induced upon methionine supplementation. Lower panel: Metabolites suppressed upon methionine supplementation. **g**, The diagram of methionine cycle is shown. **h**, **i**, CD8$^+$ T cells were cultured with fresh medium, Sup, or Sup + Met for 36 h. Metabolites related to the methionine cycle, including intracellular serine (**h**) and L-cystathionine (**i**), were detected by MS. **j**, **k**, Effect of tumour supernatants on CD8$^+$ T cell histone methylation. Mouse (**j**) or human (**k**) CD8$^+$ T cells were cultured with or without methionine (Met) for 36 h with fresh medium, CT26 and MC38 tumour supernatants (**j**), or human A375 tumour supernatants (Sup) (**k**). T cell histone marks were determined by western blots. Data are mean ± s.e.m. Information on sample sizes, experimental number, times, biological replicates, statistical tests, and *P* values is available in 'Statistics and reproducibility' (Methods).

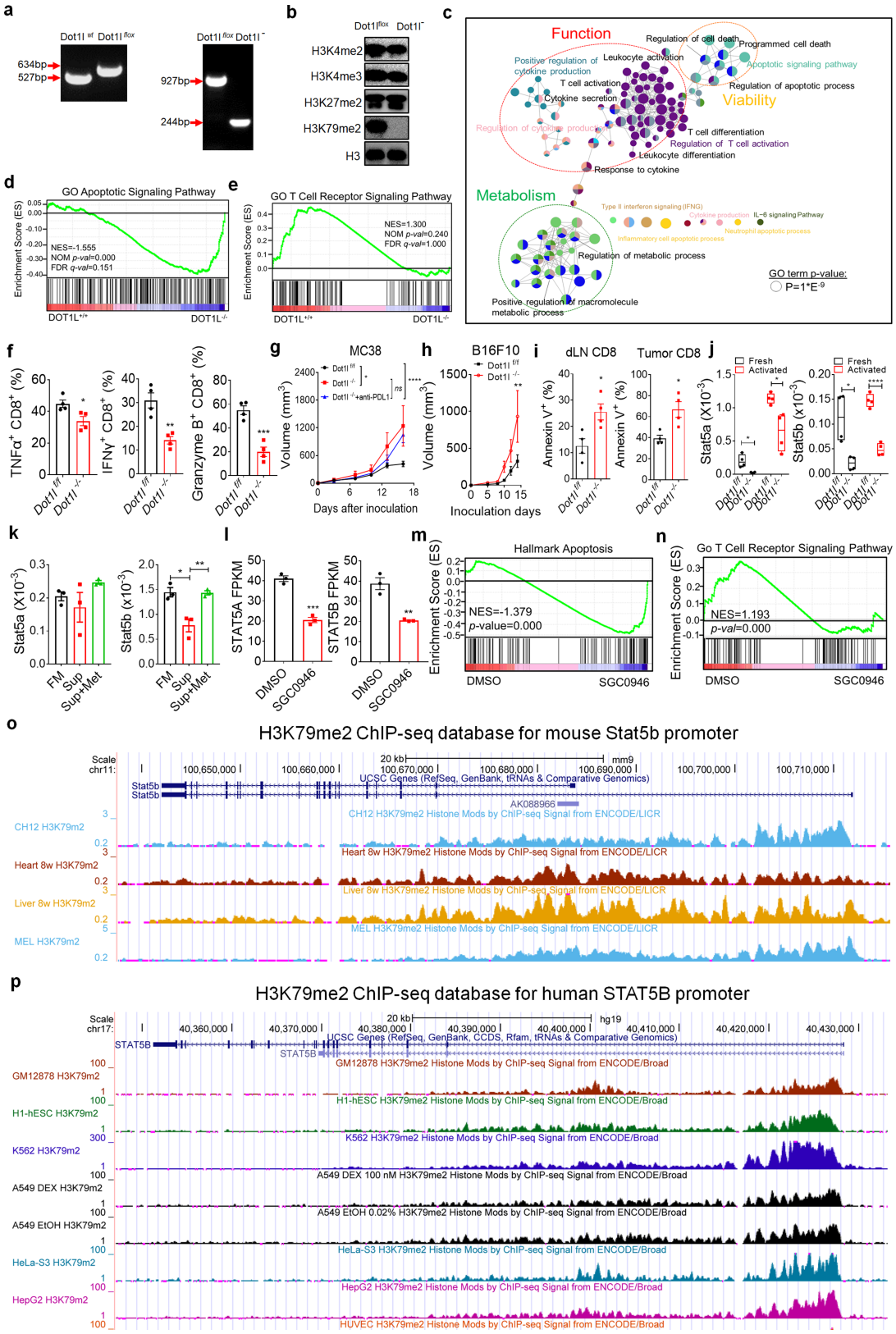

Extended Data Fig. 3 | See next page for caption.

Extended Data Fig. 3 | Loss of H3K79me2 impairs T cell anti-tumour immunity through STAT5. a, Genotyping for *Dot1l*$^{f/f}$ and *Dot1l*$^{-/-}$ mice by PCR. **b**, Effect of Dot1l knockout on histone marks in T cells. **c**-**e**, Gene signature comparison between *Dot1l*$^{-/-}$ and *Dot1l*$^{f/f}$ CD8$^+$ T cells. Functionally grouped network of enriched categories was generated for the hub genes and their regulators using ClueGO. Visualization has been carried out using Cytoscape 3.7.1. (**c**). GSEA plot showed enriched apoptotic gene pathway (**d**) and impaired TCR signalling pathway (**e**) in *Dot1l*$^{-/-}$ CD8$^+$ T cells. **f**, Effect of DOT1L deficiency on T cell function in MC38 tumour. MC38 cells were inoculated into *Dot1l*$^{f/f}$ and *Dot1l*$^{-/-}$ mice. Expression of TNFα, IFNγ, and granzyme B in tumour infiltrating CD8$^+$ T cells was determined by FACS. **g**, Effect of anti-PD-L1 on tumour growth in *Dot1l*$^{+/+}$ and *Dot1l*$^{-/-}$ mice. **h**, **i**, B16F10 cells were inoculated into *Dot1l*$^{-/-}$ and *Dot1l*$^{f/f}$ mice. Effect of T cell DOT1L deficiency on tumour growth (**h**) and T cell viability (**i**) were monitored. **j**, Real-time PCR showed *Stat5a* and *Stat5b* transcripts in fresh or anti-CD3/CD28 activated *Dot1l*$^{f/f}$ and *Dot1l*$^{-/-}$ CD8$^+$ T cells. **k**, Real-time PCR showed *Stat5a* and *Stat5b* transcripts in activated CD8$^+$ T cells cultured with fresh medium, B16F10 tumour supernatants (Sup), or supernatants plus methionine (Sup + Met) for 24 h. **l**–**n**, RNA-seq showed the effect of DOT1L inhibitor (SGC0946) on human CD8$^+$ T cells (Database: GSE108694). STAT5A and STAT5B (**l**) transcripts were quantified in human CD8$^+$ T cells treated with DOT1L inhibitor SGC0946. GSEA enrichment plot showed enrichment of apoptotic gene pathway (**m**) and defects in T cell receptor related pathways (**n**) in human CD8$^+$ T cells treated with DOT1L inhibitor. **o**, **p**, H3K79me2 ChIP-seq in ENCODE database showing *Stat5b* promoter in mice (**o**) and humans (**p**). Data are mean ± s.e.m. Information on sample sizes, experimental number, times, biological replicates, statistical tests, and *P* values is available in 'Statistics and reproducibility' (Methods).

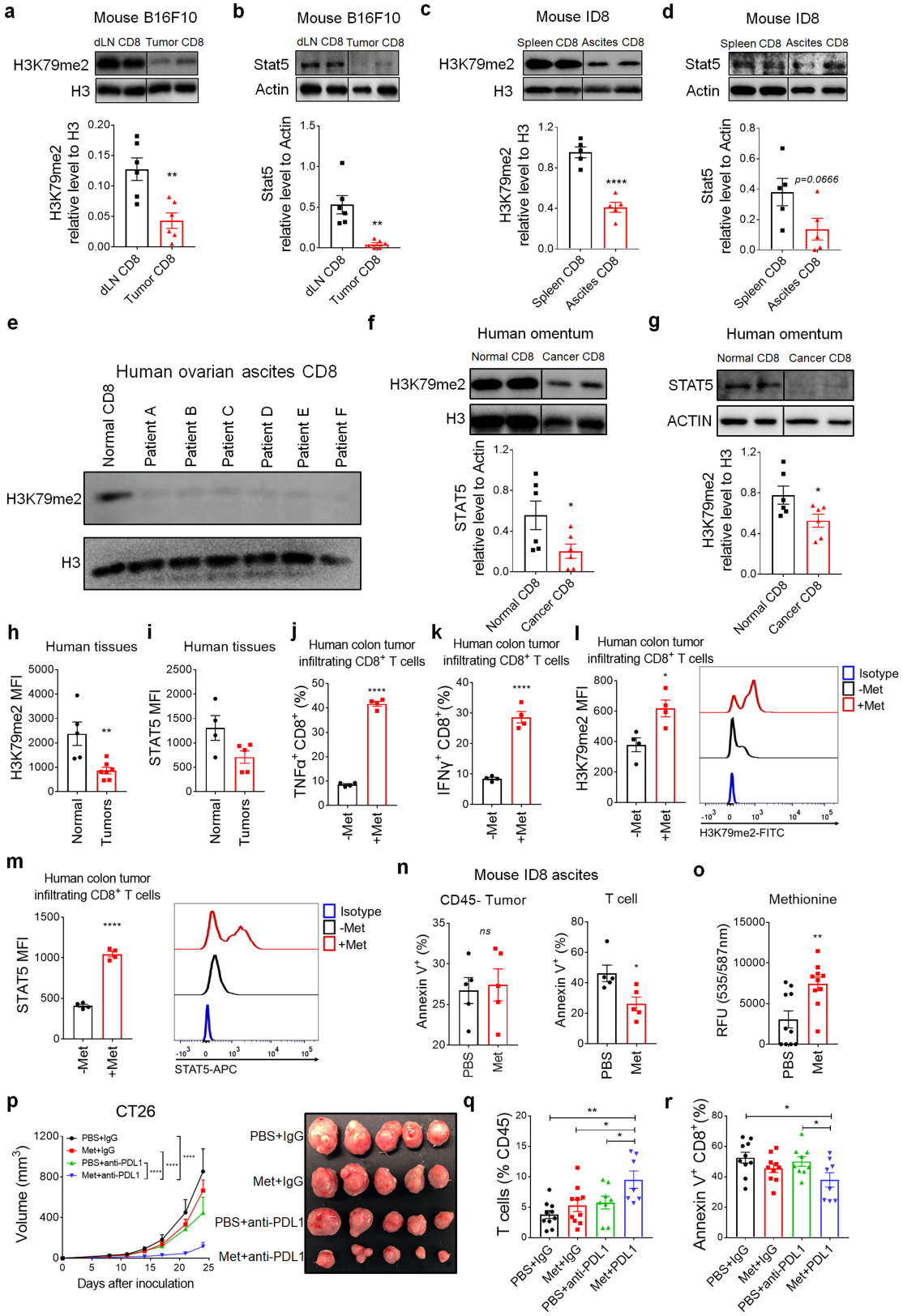

Extended Data Fig. 4 | See next page for caption.

Extended Data Fig. 4 | Methionine supplementation promotes T cell anti-tumour immunity. a, b, H3K79me2 (**a**) and STAT5 (**b**) levels in $CD8^+$ T cells from tumour draining lymph node and tumour in B16F10 bearing mice. **c, d**, H3K79me2 (**c**) and STAT5 (**d**) levels in $CD8^+$ T cells from spleen and tumour ascites in ID8 bearing mice. **e**, H3K79me2 levels in $CD8^+$ T cells from healthy peripheral blood and human ovarian cancers ascites. **f**, **g**, H3K79me2 (**f**) and STAT5 (**g**) levels in $CD8^+$ T cells from healthy human blood and human ovarian cancer omentum tissues. **h, i**, FACS showed H3K79me2 and STAT5 levels in human tumour infiltrating $CD8^+$ T cells. **j**–**m**, Effect of methionine on human tumour infiltrating $CD8^+$ T cells. Human colorectal cancer infiltrating $CD8^+$ T cells were cultured with or without methionine. T cell cytokine production (**j**, **k**), H3K79me2 (**l**), and STAT5 (**m**) were analysed by FACS. One representative of four is shown. **n**, Effect of methionine supplementation on apoptosis of tumour infiltrating $CD8^+$ T cells and ID8 tumour cells in vivo. ID8 tumour bearing mice were treated with methionine or PBS. T cell and tumour cell apoptosis was determined by FACS. **o**, Methionine levels in ID8 tumour after methionine or PBS treatment. **p**–**r**, Effect of anti-PD-L1 on methionine-affected CT26 tumour progression. Mice bearing CT26 tumour were treated with anti-PD-L1, methionine, and their combination. Tumour volume (**p**), T cell tumour infiltration (**q**) and apoptosis (**r**) were assessed. Data are mean ± s.e.m. Information on sample sizes, experimental number, times, biological replicates, statistical tests, and *P* values is available in 'Statistics and reproducibility'.

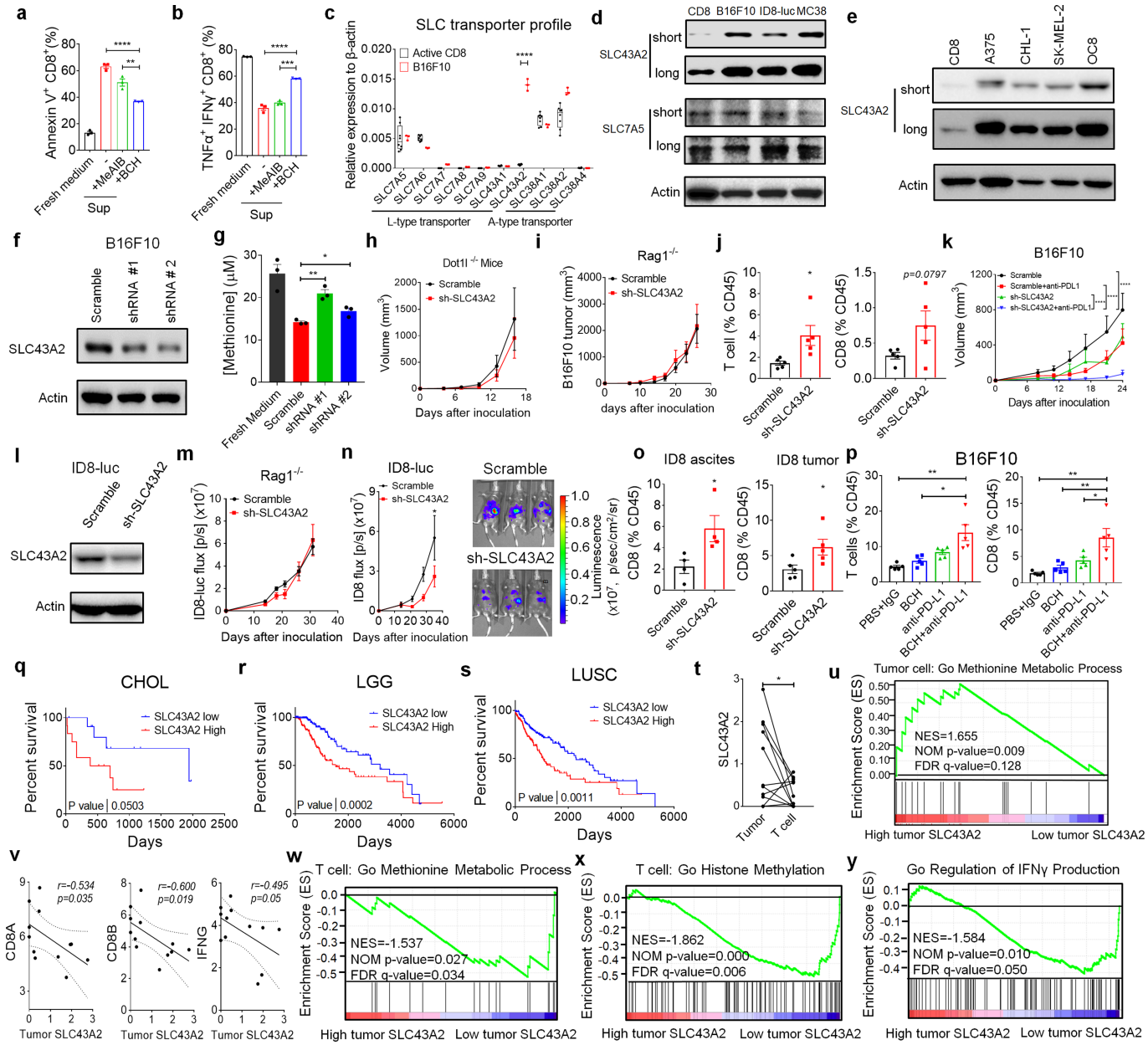

Extended Data Fig. 5 | Tumour SLC43A2 correlates to poor T cell immunity. **a, b**, Effects of SLC inhibitors (BCH or MeAIB) on tumour cell affected CD8 T cell apoptosis (**a**) and cytokine production (**b**). **c**, Real-time PCR showed SLC transporter transcripts in activated $CD8^+$ T cells and B16F10 tumour cells. **d**, Western Blot showed SLC43A2 and SLC7A5 proteins in activated $CD8^+$ T cells and tumour cells. **e**, Western Blot showed SLC43A2 protein in human $CD8^+$ T cells and human tumour cells. **f**, Western Blot showed SLC43A2 knockdown efficiency in B16F10 cells. **g**, Effect of tumour cell SLC43A2 knockdown on methionine consumption. WT (scramble) and sh-SLC43A2 tumour cells were cultured with fresh medium containing 30 μM methionine for 24 h. Methionine concentration was measured by MS in fresh medium and supernatants. **h**, Wild-type and sh-SLC43A2 B16F10 tumour growth in *Dot1l*$^{-/-}$ mice. **i**, Wild-type and SLC43A2 knockdown B16F10 tumour growth in *Rag1*$^{-/-}$ mice. **j**, Effect of tumour SLC43A2 knockdown on T cell tumour infiltration in WT or sh-SLC43A2 B16F10 bearing mice. **k**, Effect of SLC43A2 knockdown and the combination of anti-PD-L1 on B16F10 bearing mice. **l**, Western Blot showed SLC43A2 knockdown efficiency in ID8-luc cells. **m**, Wild type and SLC43A2 knockdown ID8-luc tumour growth in *Rag1*$^{-/-}$ mice. **n**, **o**, Effect of tumour SLC43A2 knockdown on ID8 growth (**n**) and T cell tumour infiltration in WT or sh-SLC43A2 ID8 bearing mice. **p**, T cell tumour infiltration in B16F10 bearing mice treated with BCH, anti-PD-L1, or their combination. **q**–**s**, Kaplan–Meier survival curves showed the prognostic values of SLC43A2 expression in different types of tumour: Cholangiocarcinoma (CHOL, **q**), low grade glioma (LGG, **r**), and lung squamous cell carcinoma (LUSC, **s**). The raw data was from TCGA. **t**–**y**, The analysis was based on single cell RNA-seq data (GSE72056). **t**, SLC43A2 transcripts were compared in tumour cells versus tumour infiltrating T cells from the same human melanoma tissues. **u**, GSEA plots showed methionine metabolic process genes in tumour cells expressing high versus low SLC43A2. **v**, Correlation was analysed between CD8A, CD8B, IFNG transcripts in T cells and SLC43A2 transcripts in tumour cells in the same human melanoma tissues. **w**-**y**, GSEA enrichment plot analysis showed defective pathways in tumour infiltrating T cells in melanoma patients with high tumour SLC43A2 compared to low tumour SLC43A2. The pathways included T cell methionine metabolic process (**w**), histone methylation (**x**), and IFNγ production (**y**). Data are mean ± s.e.m. Information on sample sizes, experimental number, times, biological replicates, statistical tests, and *P* values is available in 'Statistics and reproducibility' (Methods).

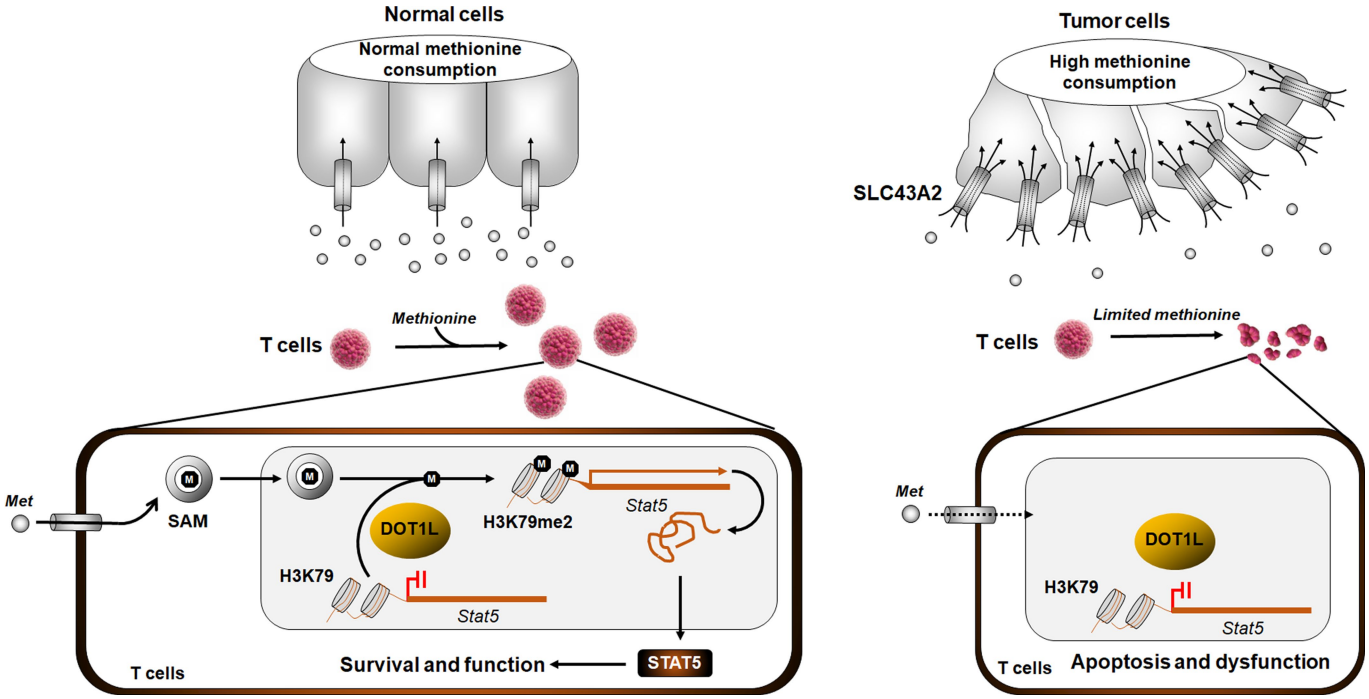

Extended Data Fig. 6 | Graphical model. Model of how tumour cells outcompete T cells for methionine and disrupt T cell survival and function.

Extended Data Table 1 | ChIP primers for mouse *Stat5b*

Site	CHIP primer region	Primer Sequence
1	Stat5b promoter #1 (-186~-369)	F: 5'-TCATTCAGTCAGGATACGGGC-3'
		R: 5'-GAATTCCCCAGCTGAAAAGGC-3'
2	Stat5b promoter #2 (-790~-930)	F: 5'-AAAGGCGAAGAACAAACGGC-3'
		R: 5'-TACAAGTTCCGACCCACAGC-3'
3	Stat5b promoter #3 (-1072~-1240)	F: 5'-GCTTGAATGTGTGGTGGTGG-3'
		R: 5'-AGACAGCTCTCCTTCCGACT-3'
4	Stat5b promoter #4 (-1072~-1240)	F: 5'- CGTGCTCCTGCTGTCTAGAAGCTGGG-3'
		R: 5'- GGGATCGGCTCTGTCGGCGTC-3'
5	Stat5b promoter #5 (-3148~-3308)	F: 5'-AGGCCAGGAGTGTGTTTCTG-3'
		R: 5'-TGGAAATCAGCAGCTCTGGG-3'
6	Stat5b promoter #6 (-3886~-3940)	F: 5'-ATAGTGGGTGGCAGGGTTTG-3'
		R: 5'-CTGTCTACCTCATGGCGTCC-3'

Extended Data Table 2 | Characteristics of patients with colorectal cancer

Number	Gender	Age	Tumor histology	Grade	Primary tumor location	Stage	TNM
1	M	62	Adenocarcinoma tubulare	G2	Sigmoid colon	III	T4N1M0
2	M	84	Adenocarcinoma tubulare	G2	Transverse colon (Hepatic flexure)	II	T3N0M0
3	F	62	Adenocarcinoma tubulare	G2	Sigmo-rectal flexure	III	T3NxM0
4	M	66	Adenocarcinoma	G2	Ceacum	IV	T4N1M1
5	M	59	Adenocarcinoma tubulare	G3	Sigmoid colon	IV	T4N1M1
6	M	81	Adenocarcinoma tubulare	G2	Sigmoid colon	II	T3N0M0
7	F	65	Adenocarcinoma	G2	Sigmoid	III	T2N0M0

Extended Data Table 3 | Primers for RT–PCR and *Dot1l* mouse genotyping

Gene	Forward Sequence (5'-3')	Reverse Sequence (5'-3')
Slc3a2	GAGCGTACTGAATCCCTAGTCAC	GCTGGTAGAGTCGGAGAAGATG
Slc7a5	GGTCTCTGTTCACGTCCTCAAG	GAACACCAGTGATGGCACAGGT
Slc7a6	TCTACCTTCGCTGGAAAGAGCC	GCCACCAGAAACAAGGAGCAGA
Slc7a7	AAGGTGTTGGCGCTGATTGCAG	AGAGTGCCAGAGCAATGTCACC
Slc7a8	GCATACGTCACTGCAATGTCCC	GGAGCCATTGACTCCACCAAAC
Slc7a9	GGATTCCTCTGGTGACCGTATG	CAAGATGCTGGATAGAGAACGCG
Slc38a1	TACCAGAGCACAGGCGACATTC	ATGGCGGCACAGGTGGAACTTT
Slc38a2	GCGTTGGCATTCAATAGCACCG	TCGTAGATGGGAAGAACAGCGG
Slc38a4	CTCTTCACAGCAATGGCGTGGA	GACCTCAGGGTGGCAGACAAAA
Slc43a1	TTCCTGTGGAGCCTTGTCACCA	CTCCACCTTCTGTCTCTGCTCA
Slc43a2	CAGCATCCTTGAGTTCCTGGTC	TGATGTAGCCGATGACAGGAGC
Stat5a	CCTGTTTGAGTCTCAGTTCAGCG	TGGCAGTAGCATTGTGGTCCTG
Stat5b	CACAGTTCAGCGTCGGTGGAAA	CTGTGGCATTGTTGTCCTGGCT
Actb	CATTGCTGACAGGATGCAGAAGG	TGCTGGAAGGTGGACAGTGAGG
Dot1L-genotype-Dot1l alleles	GCCTACAGCCTTCATCATTC	GATAGTCTCAATAATCTCA
Dot1L-genotype-confirming excision	GAAGTTCCTATTCCGAAGTT	GAACCACAGGATGCTTCAG

nature research

Corresponding author(s): Weiping Zou

Last updated by author(s): May 8, 2020

Reporting Summary

Nature Research wishes to improve the reproducibility of the work that we publish. This form provides structure for consistency and transparency in reporting. For further information on Nature Research policies, see Authors & Referees and the Editorial Policy Checklist.

Statistics

For all statistical analyses, confirm that the following items are present in the figure legend, table legend, main text, or Methods section.

n/a	Confirmed	
☐	☒	The exact sample size (*n*) for each experimental group/condition, given as a discrete number and unit of measurement
☐	☒	A statement on whether measurements were taken from distinct samples or whether the same sample was measured repeatedly
☐	☒	The statistical test(s) used AND whether they are one- or two-sided *Only common tests should be described solely by name; describe more complex techniques in the Methods section.*
☒	☐	A description of all covariates tested
☐	☒	A description of any assumptions or corrections, such as tests of normality and adjustment for multiple comparisons
☐	☒	A full description of the statistical parameters including central tendency (e.g. means) or other basic estimates (e.g. regression coefficient) AND variation (e.g. standard deviation) or associated estimates of uncertainty (e.g. confidence intervals)
☐	☒	For null hypothesis testing, the test statistic (e.g. *F*, *t*, *r*) with confidence intervals, effect sizes, degrees of freedom and *P* value noted *Give P values as exact values whenever suitable.*
☒	☐	For Bayesian analysis, information on the choice of priors and Markov chain Monte Carlo settings
☒	☐	For hierarchical and complex designs, identification of the appropriate level for tests and full reporting of outcomes
☐	☒	Estimates of effect sizes (e.g. Cohen's *d*, Pearson's *r*), indicating how they were calculated

Our web collection on statistics for biologists contains articles on many of the points above.

Software and code

Policy information about availability of computer code

Data collection	Flow cytometer BD LSRFortessa was used to run samples and data was acquired and analyzed by with FACSDiva v8.0.1 or FlowJo version 10. Epoch (BioTek) plate reader was used for requiring absorbance and data was analyzed by Gen5 software. The ID8-luc tumor growth was monitored by using the Xenogen IVIS Spectrum In Vivo Bioluminescence Imaging System (PerkinElmer). Real-time PCR was run on StepOnePlus system (Thermo fisher) and data was analyzed by StepOne Software v2.2.2. RNA-Seq data visualization has been carried out using Cytoscape v3.7.1. Data was also collected using standard software, such as Microsoft Excel 2016 and GraphPad Prism version 7.
Data analysis	GraphPad Prism version 7 was used for data analysis. FACS data were analyzed with FACSDiva v8.0.1 or FlowJo version 10. Functionally grouped network of enriched categories was generated for the hub genes and their regulators using ClueGO. RNA-Seq data visualization has been carried out using Cytoscape v3.7.1. Pathways gene enrichment were analyzed by using GSEA v4.0.3.

For manuscripts utilizing custom algorithms or software that are central to the research but not yet described in published literature, software must be made available to editors/reviewers. We strongly encourage code deposition in a community repository (e.g. GitHub). See the Nature Research guidelines for submitting code & software for further information.

Data

Policy information about availability of data

All manuscripts must include a data availability statement. This statement should provide the following information, where applicable:

- Accession codes, unique identifiers, or web links for publicly available datasets
- A list of figures that have associated raw data
- A description of any restrictions on data availability

All data supporting the results of this study are available from the corresponding author upon request.

Field-specific reporting

Please select the one below that is the best fit for your research. If you are not sure, read the appropriate sections before making your selection.

☒ Life sciences ☐ Behavioural & social sciences ☐ Ecological, evolutionary & environmental sciences

For a reference copy of the document with all sections, see nature.com/documents/nr-reporting-summary-flat.pdf

Life sciences study design

All studies must disclose on these points even when the disclosure is negative.

Sample size	No statistical method was used to calculate sample size. Sample size was determined to be adequate based on the magnitude and consistency of measurable differences between groups. The size of animal studies is between 5 to 20, which are commonly used in similar studies in literatures.
Data exclusions	No data was excluded for all in vitro experiments. No data was excluded for all in vitro experiments. We did not perform any pre-established exclusions for in vivo experiments. In in vivo survival studies we excluded small number of animals died due to other than tumor-related condition.
Replication	As reported in the figure legends, experiments were performed at least three times with similar results, the findings were reliably reproduced.
Randomization	For all in vivo experiments, animals were randomly assigned into a treatment group after tumor inoculation. The starting tumor burden in the treatment and control groups was similar before treatment.
Blinding	Investigators were not blinded to mouse genotypes during experiments. Tumor measurements were performed by person blinded to which animal was being measured.

Behavioural & social sciences study design

All studies must disclose on these points even when the disclosure is negative.

Study description	*Briefly describe the study type including whether data are quantitative, qualitative, or mixed-methods (e.g. qualitative cross-sectional, quantitative experimental, mixed-methods case study).*
Research sample	*State the research sample (e.g. Harvard university undergraduates, villagers in rural India) and provide relevant demographic information (e.g. age, sex) and indicate whether the sample is representative. Provide a rationale for the study sample chosen. For studies involving existing datasets, please describe the dataset and source.*
Sampling strategy	*Describe the sampling procedure (e.g. random, snowball, stratified, convenience). Describe the statistical methods that were used to predetermine sample size OR if no sample-size calculation was performed, describe how sample sizes were chosen and provide a rationale for why these sample sizes are sufficient. For qualitative data, please indicate whether data saturation was considered, and what criteria were used to decide that no further sampling was needed.*
Data collection	*Provide details about the data collection procedure, including the instruments or devices used to record the data (e.g. pen and paper, computer, eye tracker, video or audio equipment) whether anyone was present besides the participant(s) and the researcher, and whether the researcher was blind to experimental condition and/or the study hypothesis during data collection.*
Timing	*Indicate the start and stop dates of data collection. If there is a gap between collection periods, state the dates for each sample cohort.*
Data exclusions	*If no data were excluded from the analyses, state so OR if data were excluded, provide the exact number of exclusions and the rationale behind them, indicating whether exclusion criteria were pre-established.*
Non-participation	*State how many participants dropped out/declined participation and the reason(s) given OR provide response rate OR state that no participants dropped out/declined participation.*
Randomization	*If participants were not allocated into experimental groups, state so OR describe how participants were allocated to groups, and if allocation was not random, describe how covariates were controlled.*

Ecological, evolutionary & environmental sciences study design

All studies must disclose on these points even when the disclosure is negative.

Study description	*Briefly describe the study. For quantitative data include treatment factors and interactions, design structure (e.g. factorial, nested, hierarchical), nature and number of experimental units and replicates.*

Research sample	*Describe the research sample (e.g. a group of tagged Passer domesticus, all Stenocereus thurberi within Organ Pipe Cactus National Monument), and provide a rationale for the sample choice. When relevant, describe the organism taxa, source, sex, age range and any manipulations. State what population the sample is meant to represent when applicable. For studies involving existing datasets, describe the data and its source.*
Sampling strategy	*Note the sampling procedure. Describe the statistical methods that were used to predetermine sample size OR if no sample-size calculation was performed, describe how sample sizes were chosen and provide a rationale for why these sample sizes are sufficient.*
Data collection	*Describe the data collection procedure, including who recorded the data and how.*
Timing and spatial scale	*Indicate the start and stop dates of data collection, noting the frequency and periodicity of sampling and providing a rationale for these choices. If there is a gap between collection periods, state the dates for each sample cohort. Specify the spatial scale from which the data are taken*
Data exclusions	*If no data were excluded from the analyses, state so OR if data were excluded, describe the exclusions and the rationale behind them, indicating whether exclusion criteria were pre-established.*
Reproducibility	*Describe the measures taken to verify the reproducibility of experimental findings. For each experiment, note whether any attempts to repeat the experiment failed OR state that all attempts to repeat the experiment were successful.*
Randomization	*Describe how samples/organisms/participants were allocated into groups. If allocation was not random, describe how covariates were controlled. If this is not relevant to your study, explain why.*
Blinding	*Describe the extent of blinding used during data acquisition and analysis. If blinding was not possible, describe why OR explain why blinding was not relevant to your study.*

Did the study involve field work? ☐ Yes ☐ No

Field work, collection and transport

Field conditions	*Describe the study conditions for field work, providing relevant parameters (e.g. temperature, rainfall).*
Location	*State the location of the sampling or experiment, providing relevant parameters (e.g. latitude and longitude, elevation, water depth).*
Access and import/export	*Describe the efforts you have made to access habitats and to collect and import/export your samples in a responsible manner and in compliance with local, national and international laws, noting any permits that were obtained (give the name of the issuing authority, the date of issue, and any identifying information).*
Disturbance	*Describe any disturbance caused by the study and how it was minimized.*

Reporting for specific materials, systems and methods

We require information from authors about some types of materials, experimental systems and methods used in many studies. Here, indicate whether each material, system or method listed is relevant to your study. If you are not sure if a list item applies to your research, read the appropriate section before selecting a response.

Materials & experimental systems

n/a	Involved in the study
☐	☒ Antibodies
☐	☒ Eukaryotic cell lines
☒	☐ Palaeontology
☐	☒ Animals and other organisms
☐	☒ Human research participants
☒	☐ Clinical data

Methods

n/a	Involved in the study
☒	☐ ChIP-seq
☐	☒ Flow cytometry
☒	☐ MRI-based neuroimaging

Antibodies

Antibodies used	Antibodies used for in vivo experiments, anti-mouse PD-L1 (Clone: 10F.9G2, Catalog # BE0101) and rat IgG2b isotype (Clone: LTF-2, Catalog # BE0090) were from Bioxcell validated in our previous works (https://www.jci.org/articles/view/96113 and https://www.nature.com/articles/s41586-019-1170-y#Sec2). Antibodies for functional studies: anti-human CD3 (Clone HIT3α, BD Biosciences, Catalog No. 555336, Working concentration: 5µg/L) and anti-human CD28 (Clone CD28.2, BD Biosciences, Catalog No. 555725, Working concentration: 2.5µg/L), anti-mouse CD3 (Clone 145-2C11, BD Biosciences, Catalog No. 553057, Working concentration: 5µg/L) and anti-mouse CD28 (Clone 37.51, BD Biosciences, Catalog No. 553294, Working concentration: 2.5µg/L).

Antibodies used for FACS: anti-mouse CD45 (30-F11,Thermo Fisher Scientific, Catalog # MCD4517), anti-mouse CD90 (53-2.1, Thermo Fisher Scientific, Catalog # 11-0902-82), anti-mouse CD4 (RM4-5, Thermo Fisher Scientific, Catalog # 47-0042-82), anti-mouse CD8 (53-6.7, Thermo Fisher Scientific, Catalog # 56-0081-82), anti-mouse IL-2 (JES6-5H4, Thermo Fisher Scientific, Catalog # 17-7021-82), anti-mouse TNF (MP6-XT22, Thermo Fisher Scientific, Catalog # 25-7321-82), anti-mouse IFNγ (XMG1.2, BD Biosciences, Catalog No. 563773), anti-mouse Granzyme B (NGZB, Thermo Fisher Scientific, Catalog # 12-8898-82), PE-Cy™7 Mouse Anti-Human CD3 (Clone UCHT1, BD Biosciences, Catalog No. 563423), APC-Cy™7 Mouse Anti-Human CD8 (Clone RPA-T8, BD Biosciences, Catalog No. 557760), Pacific Blue-anti-human IFNγ (4S.B3, BD Biosciences, Catalog No. 564791), PerCP-Cy™5.5 Mouse Anti-Human IFN-γ (4S.B3, BD Biosciences, Catalog No. 560742), APC-anti-human TNF (MAb11, BD Biosciences, Catalog No. 562084), FITC-Mouse Anti-Human TNF (MAb11, BD Biosciences, Catalog No. 552889), PE Rat anti-human IL-2 (MQ1-17H12, BD Biosciences, Catalog No. 560709), Alexa Fluor® 647 Mouse anti-Human Granzyme B (GB11, BD Biosciences, Catalog NO. 560212), APC-anti-STAT5 (REA549, Miltenyi Biotec Inc., Order no: 130-108-873), 7AAD (BD Biosciences, Catalog No. 559925), FITC-Annexin V (BD Biosciences, Catalog No. 556419).

Antibodies used for immunoblot and ChIP: anti-Histone H3 (di methyl K4) antibody (Abcam, Cat# ab194678, 1:1000), anti-Histone H3 (tri methyl K4) antibody (Abcam, Cat# ab8580, 1:1000), anti-Histone H3 (di methyl K9) antibody (Abcam, Cat# ab176882, 1:1000), anti-Histone H3 (di methyl K27) antibody (Abcam, Cat# ab24684, 1:1000), anti-Histone H3 (di methyl K79) antibody (Abcam, Cat# ab3594, 1:1000), anti-Histone H3 (tri methyl K79) antibody (Abcam, Cat# ab2621, 1:1000), anti-Histone H3 Antibody (Cell Signaling Technology, Cat# 9715, 1:1000), anti- STAT1 (Cell Signaling Technology, Cat# 14994, 1:1000), anti-STAT3 (Cell Signaling Technology, Cat# 12640, 1:1000), anti- STAT5 (Cell Signaling Technology, Cat# 94205, 1:1000), anti-Phospho-STAT5 (Tyr694) (Cell Signaling Technology, Cat# 4322, 1:1000), Normal Rabbit IgG (Cell Signaling Technology, Cat# 2729, 1:1000), anti-β-Actin (Antibody Cell Signaling Technology, Cat# 4967, 1:1000), anti-SLC43A2 antibody (Abcam, Cat# ab107426, 1:1000), anti-SLC7A5 Polyclonal Antibody (Invitrogen, Cat# PA5-50485, 1:1000).

Validation

All antibodies for FACS and western blot were well-recognized clones in the field and validated by the manufacturers. These antibodies are further validated and routinely used in our lab.
Antibodies targeting SLC43A2 were validated by knockdown through MISSION shRNA (Sigma) and the GIPZ Lentiviral shRNA systems, and verification of the decrease of a band of the predicted molecular weight by immunoblotting.

Eukaryotic cell lines

Policy information about cell lines

Cell line source(s)

Human cells (including A375, CHL-1, SK-MEL-2, 293T cells) and mouse tumor cells (including B16F10 and CT26 cells) were obtained from ATCC. Mouse ID8-luc and MC38 cells and human primary high grade serous ovarian carcinoma cells (OC8) are cited.

Authentication

STR fingerprint analysis

Mycoplasma contamination

All cell lines in our laboratory are routinely tested for mycoplasma contamination and cells used in this study are negative for mycoplasma.

Commonly misidentified lines
(See ICLAC register)

No cell line used in the paper is listed in ICLAC database.

Palaeontology

Specimen provenance

Provide provenance information for specimens and describe permits that were obtained for the work (including the name of the issuing authority, the date of issue, and any identifying information).

Specimen deposition

Indicate where the specimens have been deposited to permit free access by other researchers.

Dating methods

If new dates are provided, describe how they were obtained (e.g. collection, storage, sample pretreatment and measurement), where they were obtained (i.e. lab name), the calibration program and the protocol for quality assurance OR state that no new dates are provided.

☐ Tick this box to confirm that the raw and calibrated dates are available in the paper or in Supplementary Information.

Animals and other organisms

Policy information about studies involving animals; ARRIVE guidelines recommended for reporting animal research

Laboratory animals

Six- to eight-week-old female wild-type C57BL/6, BALB/c, and Rag1 knock out (KO) mice were from the Jackson Laboratory. Dot1l flox/flox mice were bred to CD4-Cre mice to generate mice with specific DOT1L deletion in T cells. All mice were maintained under pathogen-free conditions.

Wild animals

The study did not involve wild animals.

Field-collected samples

The study did not involve samples collected from field.

Ethics oversight

University Committee on the Use and Care of Animals at the University of Michigan

Note that full information on the approval of the study protocol must also be provided in the manuscript.

Human research participants

Policy information about studies involving human research participants

Population characteristics	Colorectal cancer (stage from II to IV) patients were recruited for the methionine supplementation study. There are 5 males and 2 females, with the age range from 59-84 (average 68.4).
Recruitment	None selection had been made, every patient who meet the eligibility criteria were selected for study.
Ethics oversight	This study was conducted according to the Declaration of Helsinki and approved by the institutional review board, with written informed consent obtained from all patients.

Note that full information on the approval of the study protocol must also be provided in the manuscript.

Clinical data

Policy information about clinical studies

All manuscripts should comply with the ICMJE guidelines for publication of clinical research and a completed CONSORT checklist must be included with all submissions.

Clinical trial registration	*Provide the trial registration number from ClinicalTrials.gov or an equivalent agency.*
Study protocol	*Note where the full trial protocol can be accessed OR if not available, explain why.*
Data collection	*Describe the settings and locales of data collection, noting the time periods of recruitment and data collection.*
Outcomes	*Describe how you pre-defined primary and secondary outcome measures and how you assessed these measures.*

ChIP-seq

Data deposition

☐ Confirm that both raw and final processed data have been deposited in a public database such as GEO.

☐ Confirm that you have deposited or provided access to graph files (e.g. BED files) for the called peaks.

Data access links *May remain private before publication.*	*For "Initial submission" or "Revised version" documents, provide reviewer access links. For your "Final submission" document, provide a link to the deposited data.*
Files in database submission	*Provide a list of all files available in the database submission.*
Genome browser session (e.g. UCSC)	*Provide a link to an anonymized genome browser session for "Initial submission" and "Revised version" documents only, to enable peer review. Write "no longer applicable" for "Final submission" documents.*

Methodology

Replicates	*Describe the experimental replicates, specifying number, type and replicate agreement.*
Sequencing depth	*Describe the sequencing depth for each experiment, providing the total number of reads, uniquely mapped reads, length of reads and whether they were paired- or single-end.*
Antibodies	*Describe the antibodies used for the ChIP-seq experiments; as applicable, provide supplier name, catalog number, clone name, and lot number.*
Peak calling parameters	*Specify the command line program and parameters used for read mapping and peak calling, including the ChIP, control and index files used.*
Data quality	*Describe the methods used to ensure data quality in full detail, including how many peaks are at FDR 5% and above 5-fold enrichment.*
Software	*Describe the software used to collect and analyze the ChIP-seq data. For custom code that has been deposited into a community repository, provide accession details.*

Flow Cytometry

Plots

Confirm that:

☒ The axis labels state the marker and fluorochrome used (e.g. CD4-FITC).

☒ The axis scales are clearly visible. Include numbers along axes only for bottom left plot of group (a 'group' is an analysis of identical markers).

☒ All plots are contour plots with outliers or pseudocolor plots.

☒ A numerical value for number of cells or percentage (with statistics) is provided.

Methodology

Sample preparation	For cell apoptosis analysis, cells were treated, collected and rinsed with 1x binding buffer, and then stained with Annexin V and 7AAD in binding buffer at 4°C for 10 mins and directly run on a flow cytometer. To quantify T cell and cytokine production, single-cell suspensions were prepared from fresh tumor tissues and lymphocytes were enriched by density gradient centrifugation. For cytokine staining, lymphocytes were incubated in culture medium containing PMA (5 ng/ml), Ionomycin (500 ng/ml), Brefeldin A (1: 1000) and Monensin (1: 1000) at 37°C for 4 hours. Anti-CD45 (30-F11), anti-CD90 (53-2.1), anti-CD4 (RM4-5) and anti-CD8 (53-6.7) were added for 20 minute for surface staining. The cells were then washed and resuspended in 1 ml of freshly prepared Fix/Perm solution (BD Biosciences) at 4°C for overnight. After being washed with Perm/Wash buffer (BD Biosciences), the cells were stained with anti-IL-2 (JES6-5H4), anti-TNFa (MP6-XT22), anti-IFNg (XMG1.2) and anti-granzyme B (NGZB) for 30 min. For STAT5, cells were stained with APC-anti-STAT5 (REA549, Miltenyi Biotec Inc., Bergisch Gladbach, Germany). For DOT1L and H3K79me2 intracellular staining, the cells were first stained with DOT1L or H3K79me2 antibodies (Abcam), and then stained using a FITC-conjugated goat anti-rabbit IgG (H+L) secondary antibody (Invitrogen).
Instrument	All samples were acquired on BD LSRFortessa.
Software	All data were analyzed with FACS DIVA software v. 8.0 (BD Biosciences), or FlowJo V10 (LLC).
Cell population abundance	When cells were sorted or enriched, the purity was confirmed by flow cytometry and in each case was above 90% purity.
Gating strategy	The cells were gated on FSC-A/SSC-A basis on the location known to contain lymphoid cells and tumor cells. To analyze cytokine production by mouse T cells, CD45+ CD90+ population was first gated, and CD8+ and CD4+ populations were then gated. In CD8 gate, the percentage of IL-2, TNFa+, IFNg+ or Granzyme B cells were analyzed. To analyze cytokine production by human T cells, CD3+ population was first gated, and CD8+ population were then gated. The percentage of IL-2, TNFa+, IFNg+ cells were then analyzed.

☒ Tick this box to confirm that a figure exemplifying the gating strategy is provided in the Supplementary Information.

Magnetic resonance imaging

Experimental design

Design type	*Indicate task or resting state; event-related or block design.*
Design specifications	*Specify the number of blocks, trials or experimental units per session and/or subject, and specify the length of each trial or block (if trials are blocked) and interval between trials.*
Behavioral performance measures	*State number and/or type of variables recorded (e.g. correct button press, response time) and what statistics were used to establish that the subjects were performing the task as expected (e.g. mean, range, and/or standard deviation across subjects).*

Acquisition

Imaging type(s)	*Specify: functional, structural, diffusion, perfusion.*
Field strength	*Specify in Tesla*
Sequence & imaging parameters	*Specify the pulse sequence type (gradient echo, spin echo, etc.), imaging type (EPI, spiral, etc.), field of view, matrix size, slice thickness, orientation and TE/TR/flip angle.*
Area of acquisition	*State whether a whole brain scan was used OR define the area of acquisition, describing how the region was determined.*

Diffusion MRI ☐ Used ☐ Not used

Preprocessing

Preprocessing software

Provide detail on software version and revision number and on specific parameters (model/functions, brain extraction, segmentation, smoothing kernel size, etc.).

Normalization

If data were normalized/standardized, describe the approach(es): specify linear or non-linear and define image types used for transformation OR indicate that data were not normalized and explain rationale for lack of normalization.

Normalization template

Describe the template used for normalization/transformation, specifying subject space or group standardized space (e.g. original Talairach, MNI305, ICBM152) OR indicate that the data were not normalized.

Noise and artifact removal

Describe your procedure(s) for artifact and structured noise removal, specifying motion parameters, tissue signals and physiological signals (heart rate, respiration).

Volume censoring

Define your software and/or method and criteria for volume censoring, and state the extent of such censoring.

Statistical modeling & inference

Model type and settings

Specify type (mass univariate, multivariate, RSA, predictive, etc.) and describe essential details of the model at the first and second levels (e.g. fixed, random or mixed effects; drift or auto-correlation).

Effect(s) tested

Define precise effect in terms of the task or stimulus conditions instead of psychological concepts and indicate whether ANOVA or factorial designs were used.

Specify type of analysis: ☐ Whole brain ☐ ROI-based ☐ Both

Statistic type for inference
(See Eklund et al. 2016)

Specify voxel-wise or cluster-wise and report all relevant parameters for cluster-wise methods.

Correction

Describe the type of correction and how it is obtained for multiple comparisons (e.g. FWE, FDR, permutation or Monte Carlo).

Models & analysis

n/a	Involved in the study
☐	☐ Functional and/or effective connectivity
☐	☐ Graph analysis
☐	☐ Multivariate modeling or predictive analysis

Functional and/or effective connectivity

Report the measures of dependence used and the model details (e.g. Pearson correlation, partial correlation, mutual information).

Graph analysis

Report the dependent variable and connectivity measure, specifying weighted graph or binarized graph, subject- or group-level, and the global and/or node summaries used (e.g. clustering coefficient, efficiency, etc.).

Multivariate modeling and predictive analysis

Specify independent variables, features extraction and dimension reduction, model, training and evaluation metrics.